LIBRARY
JUN 24 1955

GEOCHIMICA ET COSMOCHIMICA ACTA

EDITORIAL ADVISORY BOARD

L. H. AHRENS-CAMBRIDGE, MASS · T. BARTH-OSLO · N. L. BOWEN-WASHINGTON, D. C. · A. F. BUDDINGTON-PRINCETON, N. J. · L. CAPDECOMME-TOULOUSE · E. J. CONWAY-DUBLIN · P. ESKOLA-HELSINKI · P. GALLITELLI-MODENA · J. GOGUEL-PARIS · D. GUIMARÃES-BELO HORIZONTE · A. HADDING-LUND · O. HAHN-GÖTTINGEN · H. W. HARVEY-PLYMOUTH · F. HEIDE-JENA · A. HOLMES-EDINBURGH · G. E. HUTCHINSON-NEW HAVEN, CONN. · W. Q. KENNEDY-LEEDS · PH. H. KUENEN-GRONINGEN · S. LANDERGREN-STOCKHOLM · F. MACHATSCHKI-VIENNA · B. H. MASON-BLOOMINGTON, IND. · A. MUIR-HARPENDEN · P. NIGGLI-ZÜRICH · J. ORCEL-PARIS · K. RANKAMA-HELSINKI · E. REINHARD-BASLE · TH. G. SAHAMA-HELSINKI · C. E. TILLEY-CAMBRIDGE · H. C. UREY-CHICAGO · T. VOGT-TRONDHEIM · W. WAHL-HELSINKI · T. WATANABE-TOKYO · F. WHIPPLE-CAMBRIDGE, MASS. · R. WILDT-NEW HAVEN, CONN.

EDITORS

C. W. CORRENS, GÖTTINGEN
E. INGERSON, WASHINGTON
S. R. NOCKOLDS, CAMBRIDGE
F. A. PANETH, DURHAM
L. R. WAGER, OXFORD
F. E. WICKMAN, STOCKHOLM

VOL. 2 NO. 3
1952

PERGAMON PRESS LTD · LONDON

Geochim. et Cosmochim. Acta

GEOCHIMICA ET COSMOCHIMICA ACTA

EDITORS

PROF. C. W. CORRENS, *Sedimentpetrographisches Institut der Universität, Lotzestr. 13, Göttingen, British Zone, Germany.*

DR. E. INGERSON, *United States Department of the Interior, U. S. Geological Survey, Washington 25, D. C., U.S.A.*

DR. S. R. NOCKOLDS, *Department of Mineralogy and Petrology, The University, Cambridge, England.*

PROF. F. A. PANETH, F. R. S., *Londonderry Laboratory for Radiochemistry, The University, South Road, Durham, England.*

PROF. L. R. WAGER, F.R.S., *Department of Geology and Mineralogy, The University, Oxford, England.*

PROF. F. E. WICKMAN, *Naturhistoriska Riksmuseets, Mineralogiska Avdelning, Stockholm 50, Sweden.*

1952 VOLUME 2 NUMBER 3

CONTENTS

Page

L. W. AHRENS: The use of ionization potentials. Part I.—Ionic radii of the elements 155

RIAD A. HIGAZY: Behaviour of the trace elements in a front of metasomatic-metamorphism in the Dalradian of Co. Donegal 170

D. M. SHAW: The geochemistry of indium 185

H. VON ECKERMANN, H. VON UBISCH and FRANS E. WICKMAN: A preliminary investigation into the isotopic composition of carbon from some alkaline intrusion. 207

Publishing Offices: 2, 3 & 5 Studio Place, Kinnerton Street, London S.W. 1 (SLOane 8157–9).
Subscription per volume (including postage) £ 4 4s. (U.S.A. $ 11·80). *Distributors:* All countries except U.S.A. and Germany — *Lange, Maxwell & Springer Ltd., 41–45 Neal Street, London W.C. 2.*
U.S.A. — *Academic Press Inc., 125 East 23rd Street, New York 10, N.Y.*
Germany — *Lange & Springer, Reichpietschufer 20, Berlin W 35.*

PERGAMON PRESS LTD., 2, 3 & 5 STUDIO PLACE, KINNERTON STREET, LONDON S.W. 1

Geochimica et Cosmochimica Acta, 1952, Vol. 2, pp. 155 to 169. Pergamon Press Ltd., London

The use of ionization potentials

Part 1. Ionic radii of the elements

L. H. Ahrens

Department of Geology, Massachusetts Institute of Technology

(Received 22 October 1951)

ABSTRACT

Regularities between radius, ionization potential and charge indicate strongly that in normal isoelectronic sequences, Pauling type radii (univalent set) are to be recommended over those based entirely on interionic distance measurements. Discrepancies may be caused either by error in the assumed value of the radius of O^{2-}, variable polarization and consequent shrinkage of O^{2-} and other anions, or occasionally, by lack of precision of interionic distance measurements.

Hitherto unknown radii of Ag^{2+}, At^{7+}, Au^{3+}, Br^{5+}, Cl^{5+}, Cu^{2+}, Fr^{+}, Ge^{2+}, I^{5+}, N^{3+}, Np^{7+}, P^{3+}, Pa^{5+}, Pd^{2+}, Po^{6+}, Pt^{2+}, Re^{7+}, S^{4+}, Se^{4+}, Sn^{2+}, Tc^{7+}, U^{6+} and V^{2+} are given, and all previously published radii are reviewed and revised with the aid of the regularities noted above and available interionic distance measurements.

Considerable evidence supports a value of 1,40 Å for the radius of O^{2-} when not significantly polarized.

General Introduction

The ionization potential (I) of an element may be regarded as the energy required to ionize it to a given valence state. It is thus a measure of the force of attraction between nucleus and outer electron. In this paper, the first of two in the use of ionization potentials, properties of ions such as radius are considered. In the second paper *anion affinity* and polarizing power are related to the magnitude of the ionization potential.

Ionization potentials are usually obtained spectroscopically by determining the convergence limit in a series. Determined thus they are obtained with a high degree of accuracy and are commonly expressed in volts, cm^{-1} or other units; volts are used here.

When attempting to use ionization potentials in the various ways discussed hereafter, particularly in Part 2, it is of interest to take into account the differences of environment in which ionization potentials are determined and those in which they are applied. Excitation and ionization take place by particle impact in the vapour of a discharge source where atoms and ions are relatively free, whereas ionization potentials are applied in a totally different environment—for example, the use of the ionization potential as a measure of anion affinity and polarizing power in a crystal.

Ionization potentials used here are those required to give the particular valence state in question;

for example,	Na^{+}	1st ionization potential
	Zn^{2+}	2nd ionization potential
	V^{5+}	5th ionization potential

and so on.

Ionic radii are used for many purposes. Usually one of two sets of radii are employed, either that of Goldschmidt [1] or the "univalent" set of Pauling [2];

for other sets, see Zachariasen [3] and Wyckoff [4]*. Crystallographers, mineralogists, geochemists and geologists usually employ the Goldschmidt set, whereas chemists are inclined to favour Pauling radii. Although the two sets of radii show reasonably good agreement, several important differences exist (Pauling [5], p. 350).

The discussion on the use of ionization potentials in Part 1 has three main objects; first, to show regularities between ionic radius, ionization potential and charge, and in so doing show that for ions in normal isoelectronic sequences, Pauling-type radii are to be recommended over those based entirely on interionic distance measurements; second, to utilize the ionization potential for determining some hitherto unknown radii; and third, to review and revise all published radii of ions other than those in normal isoelectronic sequences.

Resumé on Published Sets of Radii

Ionic radii listed by Goldschmidt are based on measured interionic distances in crystals which are structurally ionic. Interionic distance measurements used were mainly those given by Wyckoff [6] and in part those made by Goldschmidt, Barth, and Zachariasen (see Goldschmidt [1]). A large proportion of compounds were oxides and cation radii were obtained by subtracting an O^{2-} radius of 1·32 Å (Wasastjerna [7]) from the measured cation-anion separation. Some compounds were fluorides and in these a radius of $F^{-}=1{\cdot}33$ Å (also after Wasastjerna [7]) was used to obtain cation radii. Several radii were obtained by interpolation: for example,

$$Sc^{3+},\ Y^{3+},\quad \text{and}\quad La^{3+}.$$

It is quite clear from Goldschmidts writings that several of the radii (Si^{4+} p. 36; Al^{3+} p. 28 and some others) are very approximate. Because of common use for many years, however, all these radii are frequently regarded as accurate and cognizance is rarely taken of the approximate nature of many of them. Goldschmidt radii, like other sets, are for 6-fold co-ordination. Change of radius with change of co-ordination will not be discussed here, and the reader may refer to Pauling ([5], pp. 367–368) and other sources (see Evans [8]) for a discussion of this topic.

Wyckoff [4] gives a set of radii derived in much the same way as that of Goldschmidt. Because of its recent publication, this set contains radii based on recent interionic distance measurements. Wyckoff used an O^{2-} radius of 1·40 Å for obtaining his set, and evidence discussed below supports this value rather than 1·32 Å for the radius of O^{2-} when not seriously polarized.

The "univalent" set of ionic radii given by Pauling [2] is derived in two steps. The radius of the head member—Li^{+}, Na^{+}, K^{+}, Rb^{+}, and Cs^{+}—in each isolectronic sequence is determined from interionic distance measurements in alkali metal compounds. Once these are known, radii in each isoelectronic sequence are obtained from the inverse relationship,

$$r \propto \frac{1}{Z_{\text{eff}}}.$$

* Since submitting this paper for publication my attention has been drawn to a recent set of radii given by K. Stockar, Helv. Chim. Acta 1950 **33** 1409.

where Z_{eff} is the effective nuclear charge. The effective nuclear charge is equal to the actual nuclear charge minus the amount of electronic screening and for a given isoelectronic sequence the above equation may be written as,

$$r = \frac{K}{Z - S},$$

where S is the screening constant for each ion. A set of such screening constants has been obtained in part by theoretical calculation (PAULING [2]) and in part by interpretation of observed mole refraction and x-ray term values (PAULING and SHERMAN [9]). It should be noted that only radii of ions in normal isoelectronic sequences may be determined with the aid of the above equation.

Within an isoelectronic sequence, ionic radius should vary regularly with ionization potential and with charge. Such regularities are best displayed graphically by using log-log co-ordinates. Before showing such plots it will be necessary to revise a few of the radii of the alkali metals, because as noted, radii obtained with the aid of the above equation depend on the accuracy with which the alkali metal radii are known. If the radius of an alkali metal ion is in error, all ions in the same isoelectronic sequence carry the same systematic error. Most of the changes made below are minor, with the exception of the radius of Li^+.

Ionic Radii of the Alkali Metals

Interionic distance measurements in alkali metal halide crystals are given by WYCKOFF [4]. These values, essentially the same as used by GOLDSCHMIDT [1] are used to determine alkali metal radii, using anion radii of $F^-=1{\cdot}33$ Å (primary standard), $Cl^-=1{\cdot}81$ Å, $Br^-=1{\cdot}96$ Å and $I^-=2{\cdot}20$ Å.

Radius of Li^+.—Li^+ radii calculate as follows:

0·68 Å from Li—F
0·76 Å from Li—Cl
0·78 Å from Li—Br
0·82 Å from Li—I

The calculated radius increases when going from F to I, and at the same time there is a progressive deviation from truly ionic bonding. Only in LiF is the bonding essentially ionic, and the value of 0·68 Å is recommended.

In his discussion on alkali metal ionic radii, GOLDSCHMIDT ([1], p. 17) gave no reason for rejecting the Li—F value. His much used radius of 0·78 Å is evidently based on agreement between Li—Cl and Li—Br values, although he does not state this. WYCKOFF [4] and ZACHARIASEN [3] give a radius of 0·68 Å for Li^+.

PAULING [2] used a radius of 0·60 Å for Li^+, based on a subtraction of 1·40 Å for O^{2-} from a measured Li—O distance of 2·00 Å in Li_2O. The Li—F value is preferred because O^{2-} is more easily polarized than F^- and because Li_2O has the anti-fluorite structure, whereas the alkali metal halides (some Cs salts excepted) have the NaCl structure.

The use of $Li^+=0{\cdot}68$ Å in place of 0·60 Å introduces a systematic increase of 14 % for PAULING radii of Be^{2+}, B^{3+}, C^{4+}, N^{5+}, O^{6+}, and F^{7+}.

Radius of Na^+.—Na^+ radii calculate as follows:

0·98 Å from Na—F
1·00 Å from Na—Cl
1·01 Å from Na—Br
1·03 Å from Na—I

GOLDSCHMIDT (p. 17) chose the value of 0·98 Å. Partial transition to homopolar bonding in NaCl, NaBr, and particularly NaI, as evidenced by molecular refraction studies (FAJANS and JOOS [10]; FAJANS [11]) support the use of the Na—F value. PAULING used a value of 0·95 Å which he obtained by dividing a Na—F distance of 2·31 Å by the inverse square ratio of the effective nuclear charges of Na^+ and F^- (given as 6·48 e and 4·48 e respectively). The inverse square relationship between I and r (see below) gives a value intermediate between 0·95 Å and 0·98 Å. The mean (0·97 Å) of all values is used here and introduces a small systematic increase in radii of the sequence Na^+—Mg^{2+}—Al^{3+}—Si^{4+}—P^{5+}—S^{6+}—Cl^{7+}, over those given by PAULING.

Radii of K^+, Rb^+ *and* Cs^+

Radii given below for these ions are very similar to those listed by GOLDSCHMIDT [1], PAULING [2] and ZACHARIASEN [3]. They are based on the same interionic distance measurements used by these authors and on the use of the inverse square relationship between I and r discussed below. Radii are: $K^+ = 1{\cdot}33$ Å, $Rb^+ = 1{\cdot}47$ Å and $Cs = 1{\cdot}67$ Å.

Table 1 gives revised PAULING radii; these are used in Fig. 1, 2, 4 and 5.

Table 1. Radii (Å) *for ions in normal isoelectronic sequences (after* PAULING [2] *with revisions)*

Li^+ 0·68	Be^{2+} 0·35	B^{3+} 0·23	C^{4+} 0·16	N^{5+} 0·13	O^{6+} 0·10	F^{7+} 0·08
Na^+ 0·97	Mg^{2+} 0·66	Al^{3+} 0·51	Si^{4+} 0·42	P^{5+} 0·35	S^{6+} 0·30	Cl^{7+} 0·27
K^+ 1·33	Ca^{2+} 0·99	Sc^{3+} 0·81	Ti^{4+} 0·68	V^{5+} 0·59	Cr^{6+} 0·52	Mn^{7+} 0·46
Cu^+ 0·96	Zn^{2+} 0·74	Ga^{3+} 0·62	Ge^{4+} 0·53	As^{5+} 0·46	Se^{6+} 0·42	Br^{7+} 0·39
Rb^+ 1·47	Sr^{2+} 1·12	Y^{3+} 0·92	Zr^{4+} 0·79	Nb^{5+} 0·69	Mo^{6+} 0·62	
Ag^+ 1·26	Cd^{2+} 0·97	In^{3+} 0·81	Sn^{4+} 0·71	Sb^{5+} 0·62	Te^{6+} 0·56	I^{7+} 0·50
Cs^+ 1·67	Ba^{2+} 1·34	La^{3+} 1·14				
Au^+ 1·37	Hg^{2+} 1·10	Tl^{3+} 0·95	Pb^{4+} 0·84	Bi^{5+} 0·74		

Ionization potentials are given in Table 2 (after HERZBERG [12], LISITZIN [13], and HARRISON, LORD and LOOFBOUROW [14]).

Table 2. Ionization potentials (volts)

(a) Ions in normal valence states according to Periodic Table

1^+	2^+	3^+	4^+	5^+	6^+	7^+
Li 5·39	Be 18·21	B 37·9	C 64·5	N 97	O 137·4	F 184
Na 5·12	Mg 15·03	Al 28·4	Si 45·1	P 65	S 87·5	Cl 114
K 4·34	Ca 11·87	Sc 24·8	Ti 43·24	V ~ 65	Cr 96	Mn ~ 122
Cu 7·72	Zn 18	Ga 30·7	Ge 45·7	As 62·6	Se 82	Br 103·5
Rb 4·18	Sr 11·03	Y 20·5	Zr 34	Nb 52	Mo 70	Tc (95)
Ag 7·57	Cd 16·9	In 28·03	Sn 40·74	Sb 55·7	Te ~ 72	I 90·2
Cs 3·89	Ba 10	La 19·2	Hf 31	Ta 44·8	W 61	Re (79)
Au 9·22	Hg 18·8	Tl 29·8	Pb 39	Bi ~ 56	Po	At

(b) Other ions

1+	Tl 6·11									
2+	Mn 15·64	Fe 16·24	Co 17·4	Ni 18·2	Cu 20·3	Pb 15·04	Pd 19·9	Pt 19·3	Ag 22·0	Sn 14·6
3+	V ~ 26·5	Cr ~ 32·1								
4+	V ~ 48·5	Ce 36·7								

Regularities between Ionization Potential, Ionic Radius and Charge

Fig. 1 shows a plot of I vs r on log-log co-ordinates.

Several smooth regularities exist between r, I, and Z (see also Figs. 4 and 5). This is interpreted as strong evidence in support of the accuracy of Pauling type radii, as compared with radii based *entirely* on interionic distance measurements. It must be stated at once, however, that some of the regularities in Fig. 1—inverse square relationship between I and r for Mg^{2+}—Ca^{2+}—Sr^{2+}—Ba^{2+}, and smooth regularity in the sequence Rb^+—Sr^{2+}—Y^{3+}—Zr^{4+}—appear clearly if measured radii are plotted, provided radii of 1·40 Å and 1·33 Å for O^{2-} and F^- respectively, have been used in their derivation.

Table 3 shows some comparisons between radii from Table 1 and those obtained from interionic distance measurements as given by WYCKOFF [4] and GOLDSCHMIDT [1].

Agreement is very good except for Sr^{2+} where the measured radii are about 5% greater than the Table 1 radius.

Alkaline earth oxides crystallize with the NaCl structure, whereas MgF_2 has the rutile structure and CaF_2, SrF_2, BaF_2. and RaF_2, the fluorite structure. According to PAULING ([5], pp. 365 to 366) no significant correction is required when comparing radii obtained from the NaCl structure with those of the fluorite structure.

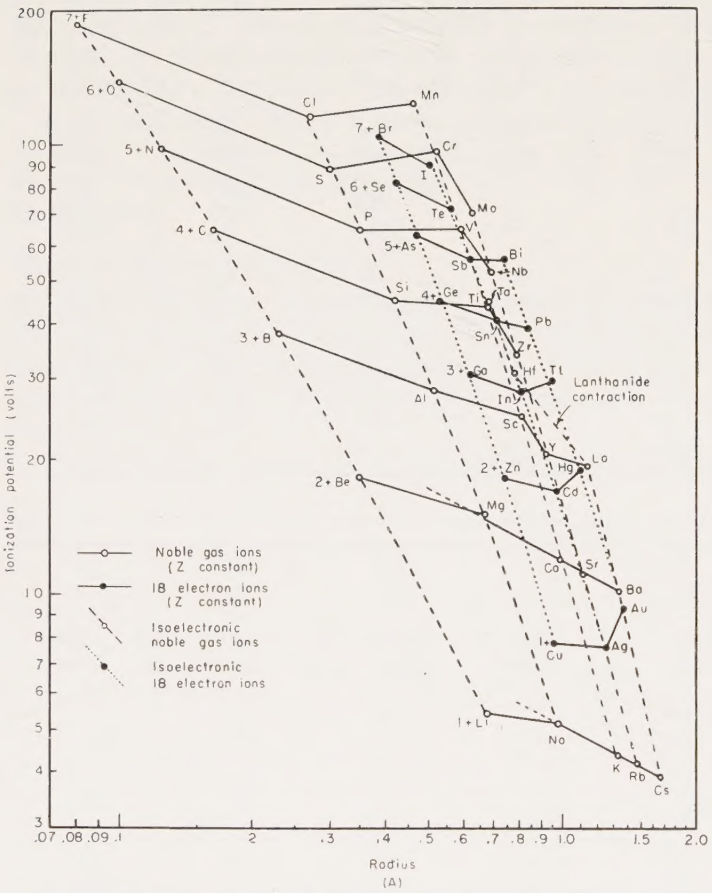

Fig. 1. Relationship between ionic radius and ionization potential, illustrating various regularities.

Agreement between Table 1 radii and those obtained from R—O and R—F interionic distance measurements supports both the accuracy of the radii given in Table 1 and a value of about 1·40 Å for the radius of O^{2-} when not seriously polarized.

Disagreement between measured and Table 1 radii becomes increasingly apparent as the polarizing power of the cation increases and causes shrinkage of O^{2-}. As a result, regularities between I, r and Z are poorly defined or completely obscured if measured radii are employed because of variable shrinkage of the anion. This applies, at least to some extent, to all 18 electron ions, and all highly charged (3+ or more) relatively small 8 electron ions. Reduction in the radius of O^{2-} may be as much as 0·05–0·15 Å even in ionic structures, as in those of Ga^{3+}, Ti^{4+}, Sn^{4+}, Pb^{4+}, Nb^{5+} and others. In non-ionic and small co-ordination number structures, shrinkage may be considerably greater. The general comments above on regularities in Fig. 1 apply much in the same way to Figs. 4 and 5. A detailed account of the relationship between I, r and Z in Fig. 1 follows.

(1) Regularities for ions of constant charge

In Fig. 1 there is a straight line relationship (slope 26–27°) between I and r for 1^+ ions Na^+—K^+– Rb^+—Cs^+, and 2^+ ions Mg^{2+}—Ca^{2+}—Sr^{2+}—Ba^{2+}; all are 8 electron ions. As tan 26–27° = 0·5, the relationship may be expressed as

$$I \propto \frac{1}{\sqrt{r}} \quad \text{or} \quad r \propto \frac{1}{I^2}.$$

For these ions therefore, an "ideal" inverse square relationship exists between radius and ionization potential.

The inverse square relationship may be utilized for checking radii of alkali metals. KCl is used as a standard crystal (see recommendation by ZACHARIASEN [3] on the use of KCl as a standard).

In the equation,

$$r = \frac{K}{I^2}$$

the constant is determined as 25·0 using $r = 1{\cdot}33$ Å and $I = 4{\cdot}32$ V for K^+. The radii of Na^+, Rb^+ and Cs^+ calculate as 0·965, 1·46 and 1·67 Å respectively, and agree very well with measured radii.

Table 3. Some comparisons of ionic radii

Ion	*R–O and R–F separations* Å	*Radius* Å	*Radius from Table 1* Å
Mg^{2+}	Mg—O : 2·10 Mg—F : 1·99	0·70 0·66	0·66
Ca^{2+}	Ca—O : 2·40 Ca—F : 2·36	1·00 1·03	0·99
Sr^{2+}	Sr—O : 2·57 Sr—F : 2·51	1·17 1·18	1·12
Ba^{2+}	Ba—O : 2·76 Ba—F : 2·68	1·36 1·35	1·34
Ra^{2+}	Ra—F : 2·77	1·44	—
Sc^{3+}	Sc—O : 2·16 2·20	0·76 0·80	0·81
Y^{3+}	Y—O : 2·32 2·38	0·94 0·98	0·92
Zr^{4+}	Zr—O : 2·19	0·79	0·79

The presence of inner electrons causes deviation from the ideal inverse square relationship. Sc^{3+} is the lightest transitional element ion, and deviation may be observed in the group Al^{3+}—Sc^{3+}—Y^{3+}—La^{3+}. This becomes progressively greater for highly charged ions and because of their abnormally high ionization potentials (see below), ions of the sequence, $Sc^3 \rightarrow Mn^{7+}$, show particularly marked deviation from an inverse square relationship between I and r.

Linearity does not exist for 18 electron ions of low charge, for example Cu^+—Ag^+ -Au^+. Gold follows entry of 4f electrons (see lanthanide contraction below) and it is not surprising that Au^+ and other 18 electron ions which follow the contraction are displaced with respect to those which precede it. The inverse square relationship does, however, appear to restore itself for highly charged 18 electron ions. This is illustrated in Fig. 2, a plot of $I\sqrt{r}$ vs. r. With the exception of Bi^{5+}, all points show a progressive trend toward restoration of the inverse square relationship which is seen in Fig. 2 to hold precisely for Se^{6+}—Te^{6+}—(Po^{6+}) and Br^{7+}—I^{7+}—(At^{7+}). Use may be made of the trend toward restoration of the inverse square relationship to determine radii of Po^{6+} and At^{7+} (see below).

(2) Regularities within isoelectronic sequences

Variation of radius with ionization potential within each isoelectronic sequence is regular without exception until entry of 4f electrons (see lanthanide contraction).

The location of the 2-electron isoelectronic sequence, $Li^+ \rightarrow F^{7+}$, is distinct from those of the 8-electron and 18-electron sequences.

The 18-electron sequence $Cu^+ \rightarrow Br^{7+}$ is located almost exactly between the two 8-electron sequences, $Na^+ \rightarrow Cl^{7+}$, and $K^+ \rightarrow Mn^{7+}$. The 18-electron sequence, $Ag^+ \rightarrow I^{7+}$, starts, however, by coinciding exactly with the 8-electron sequence $Rb^+ \rightarrow Tc^{7+}$, but gradually deviates more and more from it for highly charged ions. Likewise, the 18-electron sequence $Au^+ \rightarrow At^{7+}$ which follows entry of 4f electrons, coincides with part of the sequence, $Cs^+ \rightarrow La^{3+}$.

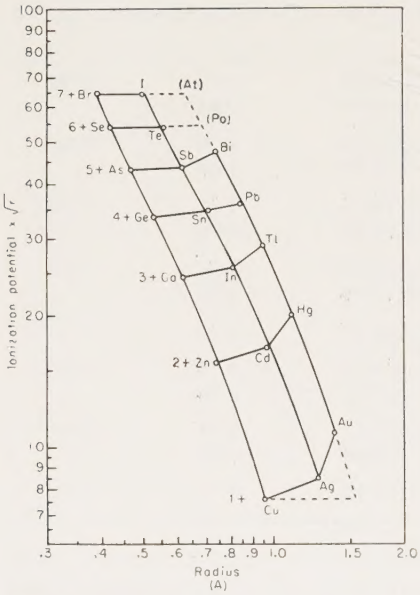

Fig. 2. Progressive trend toward restoration of the inverse square relationship between r and I (18 electron ions).

(3) The lanthanide contraction

Entry of deep-lying (4f) electrons to form rare earth elements, causes a progressive reduction in size from $La^{3+} \rightarrow Lu^{3+}$, sometimes referred to as the lanthanide contraction (VON HEVESY [15] and GOLDSCHMIDT [16]). Measurements by BOMMER [17] on C-type R_2O_3 rare earth oxides, show a radii reduction of 0·29 Å when going from $La^{3+} \rightarrow Lu^{3+}$.

Fig. 1 shows that as a result of the lanthanide contraction there is a sharp break in regularity within the sequence, $Cs^+ - Ba^{2+} - La^{3+}$ (rare earths) $- Hf^{4+} - Ta^{5+} - W^{6+} - Re^{7+}$. The locations of Hf^{4+} and Ta^{5+}, and presumably W^{6+} and Re^{7+} (data incomplete) fall along a line that is very close to the sequence $K^+ \rightarrow Mn^{7+}$.

Although entry of 4f electrons causes a reduction in size of Hf^{4+} and Ta^{5+}, and presumably W^{6+} and Re^{7+}, it does not appear to affect the usual progressive decrease in ionization potential with increase in atomic weight for 8-electron ions of constant charge. Nor does entry of 4f electrons influence linearity between charge and ionization potential as is usual when transitional elements are involved. Fig. 3a (log-log co-ordinates) shows a plot of I vs. Z for the sequence $H^+ \rightarrow N^{7+}$ (point charges) which is shown for the purpose of comparison and which appears to obey the relationship,

$$I^2 \alpha Z .$$

(Measured graphically, the value of the exponent is 1·99.) Fig. 3b shows a like plot for ions of the sequence $Na^+ \rightarrow Cl^{7+}$ (no transitional elements). The relationship is again linear but the slope is less; value of exponent $= 1{\cdot}57$. Likewise a linear relationship, not shown, exists for ions in the sequence $Li^+ \rightarrow F^{7+}$. Fig. 3c shows the effect of the entry of inner electrons; there is a break at Ca^{2+}, and for ions $Ca^{2+} \rightarrow Mn^{7+}$ the relationship is again linear. In Fig. 3d there is an equivalent break at Ba^{2+}, but entry of 4f electrons has no apparent effect on the linear relationship for ions $Ba^{2+} - La^{3+} - Hf^{4+} - Ta^{5+} - W^{6+}$: only radius breaks with I and Z after La^{3+}, as shown in Fig. 1 and 4.

18 electron ions which follow the lanthanide contraction show no reduction in size as do 8 electron ions. For example, in the group Cu^+—Ag^+—Au^+, radius increases respectively as follows; 0·95, 1·26 and 1·37 Å. However, instead of the common decrease in ionization potential with increase in atomic weight for ions of constant charge, those 18 electron elements which follow the lanthanide contraction show an increase in ionization potential. Table 4 gives two such examples:

Table 4. Ionization potentials

	Before lanthanide contraction		*After lanthanide contraction*
1^+	Cu^+ 7·72	Ag^+ 7·57	Au^+ 9·22
2^+	Zn^{2+} 18·0	Cd^{2+} 16·9	Hg^{2+} 18·8

The first ionization potential of gold is almost as great as the second of barium (Fig. 1). The increase in ionization potential for 18 electron ions which follow the lanthanide contraction becomes progressively less for highly charged ions as the inverse square relationship restores itself (Fig. 2).

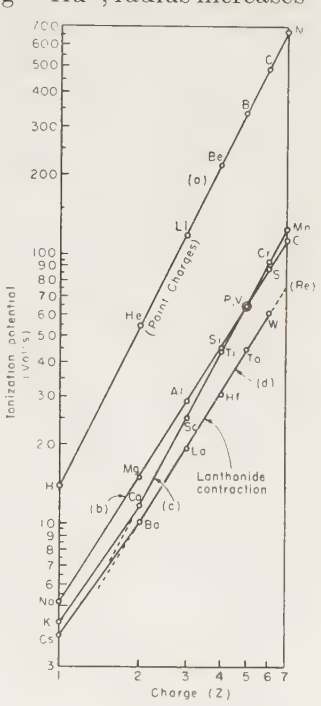

Fig. 3. Point charges obey the relationship, $I^2 \propto Z$, and ions of the sequences $Na^+ \rightarrow Cl^{7+}$ and $Li^+ \rightarrow F^{7+}$ (not shown), $I^n \propto Z$, where $n<2$. In the sequences $K^+ \rightarrow Mn^{7+}$, and $Rb^+ \rightarrow Tc^{7+}$ (not shown), breaks occur. Entry of 4f electrons (lanthanide contraction) causes no such break in the sequence $Ba^{2+} \rightarrow Re^{7+}$.

(4) Scandinide effect

Entry of inner 3d electrons causes abnormal elevation of ionization potentials for ions of the sequence $Sc^{3+} \rightarrow Mn^{7+}$. This effect becomes progressively greater for highly charged ions. Ionization potentials of V^{5+}, Cr^{6+} and Mn^{7+} are actually equal to or greater than those of lighter elements of same charge which precede them, despite the fact that in each example the ionic radius of the lighter element is smaller.

These ions violate two general rules for ions of same charge and similar configuration; first, regular decrease of ionization potential with increase in atomic weight; and second, regular decrease of ionization potential with ionic radius. Data in Table 5 illustrate abnormal behaviour of Cr^{6+}. For brevity, the exceptional behaviour of ions of the sequence $Sc^{3+} \rightarrow Mn^+$ is referred to hereafter as the "scandinide effect."

Table 5. Radii and ionization potentials for some 6^+ ions

Ion	*r* Å	*I* *(volts)*
O^{6+}	0·10	137·4
S^{6+}	0·30	87·5
Cr^{6+}	0·52	96·0
Mo^{6+}	0·62	70·0

Although ions $Sc^{3+} \rightarrow Mn^{7+}$ have abnormally high ionization potentials, their radii are not abnormally small and regular increase in ionic radius with increase in atomic weight for ions of same charge and similar configuration is not disturbed until entry of deep-lying 4f electrons (lanthanide contraction).

New and Revised Radii

(1) Radii of Hf^{4+}, Ta^{5+}, W^{6+}, Re^{7+}, Po^{6+}, Tc^{7+} *and* At^{7+}

Figs. 4 and 5 show plots (log-log co-ordinates) of ionic radius vs. charge Z for 8 electron and 18 electron ions.

Smooth regularities exist between charge and radius and these may be used in addition to the regularities in Figs. 1 and 2 to determine the radii of Hf^{4+}, Ta^{5+}, W^{6+}, Re^{7+}, Po^{6+}, At^{7+} and Tc^{7+}.

In Fig. 4 interception of the abscissa for charge 7^+ with the extrapolated curve of the sequence $Rb^+ \rightarrow Mo^{6+}$, gives a radius of 0·56 Å for Tc^{7+}. A similar value is obtained by making use of the progressive changes and regularities in Fig. 1. Use may be made of Fig. 5 in the same way for determining the radii of Po^{6+} and At^{7+} as 0·67 Å and 0·62 Å respectively. Use of the trend toward restoration of the inverse square relationship between I and r gives similar values.

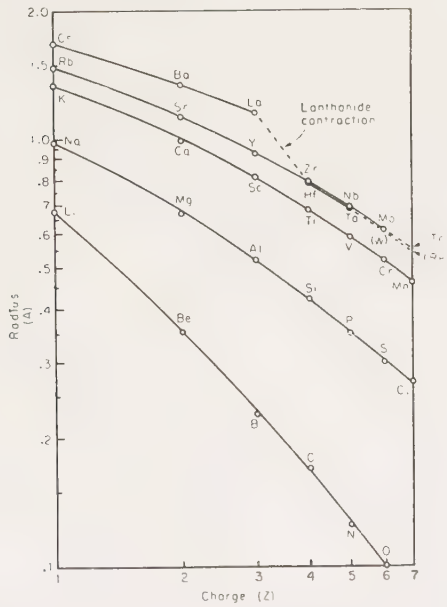

Fig. 4. Smooth regularities exist between radius and charge, except for break caused by lanthanide contraction. Extrapolation of these regularities enable determination of radii of W^{6+}, Tc^{7+} and Re^{7+}.

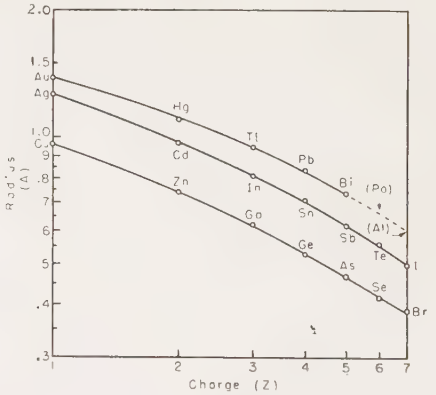

Fig. 5. Smooth regularities between Z and radius exist for 18 electron ions, and extrapolation of these regularities enable determination of radii of Po^{6+} and At^{7+}.

Pauling-type radii are not known for ions of the sequence Hf^{4+}—Ta^{5+}—W^{6+}—Re^{7+}, which follow the lanthanide contraction, but they may be determined as follows. Consider the pairs $Zr^{4+} \rightarrow Hf^{4+}$ and Nb^{5+}—Ta^{5+}. Radii of Zr^{4+} and Ta^{5+} given in Table 1 serve to calibrate interionic distance measurements in Hf and Ta compounds and the radii of Hf^{4+} and Ta^{5+} are determined as 0·78 Å and 0·68 Å. respectively.

The locations of Hf^{4+} and Ta^{5+} may now be plotted in Figs. 1 and 4. In Fig. 4 these points fall close to the curve for the sequence $Rb^+ \rightarrow Tc^{7+}$. Extrapolation of this curve gives radii of 0·62 Å and 0·56 Å for W^{6+} and Re^{7+} respectively. In Fig. 1 the plots for Hf^{4+} and Ta^{5+} fall along a curve which is apparently very close to the curve for the sequence $K^+ \rightarrow Mn^{7+}$. By employing progressive changes and

regularities in Fig. 1, similar values as those given above for W^{6+} and Re^{7+} may be obtained, but not with the same accuracy.

Radii given above are tabulated in Table 6.

(2) Radii of Fr^+ (Ac^{3+}, Th^{4+}), Pa^{5+}, U^{6+} *and* Np^{7+}

The radius of $Ra^{2+} = 1{\cdot}44$ Å is known from interionic distance measurements in RaF_2 (see measurements in Table 3, after SCHULZE [18] and may be used as a reference ion for the determination of the radii of the ions listed above. Use is made of the relationship between r and Z in Figs. 4 and 5, and a smooth curve similar in shape to that for the sequence $Rb^+ \rightarrow Tc^{7+}$, is drawn through the point for Ra^{2+}. The intercepts of this curve with abscissal values of 1, 3, 4, etc., give these radii:

$Fr^+ = 1{\cdot}80$ Å
$Ac^{3+} = 1{\cdot}18$ Å
$Th^{4+} = 1{\cdot}03$ Å
$Pa^{5+} = 0{\cdot}89$ A
$U^{6+} = 0{\cdot}80$ Å
$Np^{7+} = 0{\cdot}71$ Å

Table 6

Ion	*Radius* Å
Tc^{7+}	0·56
Po^{6+}	0·67
At^{7+}	0·62
Hf^{4+}	0·78
Ta^{5+}	0·68
W^{6+}	0·62
Re^{7+}	0·56

Radii of Ac^{3+} and Th^{4+} check those given in Tables 10 and 8 very well (1·19 and 1·02 Å respectively for Ac^{3+} and Th^{4+}) and thereby give support to the validity of the others.

(3) Radii of 3^+ *rare earth ions*

Except for La^{3+}, 3^+ rare earth radii are not given in Table 1. The Table 1 radius for La^{3+} is in excellent agreement with that obtained by subtracting an O^{2-} radius of 1·40 Å from the measured La—O distance and ionic radii of other 3^+ rare earth ions may therefore be obtained by subtracting 1·40 Å from R—O distance measurements. Table 7 gives rare earth radii obtained in this way, using measurements by BOMMER [17] on C-form R_2O_3 oxides. For measurements on La_2O_3 and Nd_2O_3 see LÖHBERG [19]. A collection of earlier measurements is given by ZACHARIASEN [20].

Table 7.
Radii of 3^+ *rare earth ions*

Element (La^{3+}	*Radius* 1·14)
Ce^{3+}	1·07
Pr^{3+}	1·06
Nd^{3+}	1·04
Sm^{3+}	1·00
Eu^{3+}	0·98
Gd^{3+}	0·97
Tb^{3+}	0·93
Dy^{3+}	0·92
(Y^{3+}	0·92)
Ho^{3+}	0·91
Er^{3+}	0·89
Tm^{3+}	0·87
Yb^{3+}	0·86
Lu^{3+}	0·85

(4) Radii of Ce^{4+}, Pr^{4+}, Tb^{4+}, Th^{4+} and U^{4+}

Agreement between the Table 1 radius of Zr^{4+} and that obtained by subtracting 1·40 Å from a Zr—O distance of 2·19 Å indicates that the same subtraction should give accurate radii of Ce^{4+}, Pr^{4+}, Tb^{4+}, Th^{4+} and U^{4+}.

Table 8 gives interionic distance measurements (GOLDSCHMIDT [1], p. 38) and ionic radii obtained by subtracting $O^{2-} = 1{\cdot}40$ Å.

If Ce^{3+} is used as a reference ion ($r = 1{\cdot}07$ Å, Table 7) in the procedure outlined below on the use of ionization potentials, a radius of 0·93 Å is obtained for Ce^{4+}; this is in good agreement with the Table 8 value.

(5) Radii of Ac^{3+}, Pa^{4+}, Np^{3+}, Np^{4+}, Pu^{3+}, Pu^{4+}, Am^{3+} *and* Am^{4+}

Zachariasen [21] has given radii of these ions based on interionic distance measurements and his method of deriving radii. His values for 3^+ and 4^+ ions of about 1 Å radius are invariably smaller than those given here. In order to make his values comparable.

Table 8. Radii of some 4^+ ions

R—O *distance*	*Radius* Å
(Zr—O: 2·19	0·79)
Ce—O: 2·34	0·94
Pr—O: 2·32	0·92
Tb—O: 2·21	0·81
Th—O: 2·42	1·02
U—O: 2·37	0·97

Table 9. Comparison of radii

Ion	Zachariasen [21]	*This publication*	*deviation* %
Th^{4+}	0·95	1·02	7
U^{4+}	0·89	0·97	8
La^{3+}	1·04	1·14	9

a correction factor of 8% has been used. This is based on a comparison (Table 9) of his radii values for Th^{4+}, U^{4+} and La^{3+}, and those given elsewhere in this publication.

Increasing Zachariasens values by 8% give the radii in Table 10.

(6) Radii of Mn^{2+}, Fe^{2+}, Co^{2+}, *and* Ni^{2+}, *and* Cr^{3+}, Fe^{3+} *and* Rh^{3+}

Table 11 gives interionic distance measurements (Wyckoff [4]) and ionic radii obtained by subtracting O^{2-}=1·40 Å and F^-=1·33 Å. Oxides have the NaCl structure and fluorides that of rutile.

Table 10

Ion	*Radius* Å
Ac^{3+}	1·19
Pa^{4+}	0·98
Np^{3+}	1·10
Np^{4+}	0·95
Pu^{3+}	1·08
Pu^{4+}	0·93
Am^{3+}	1·07
Am^{4+}	0·92

Table 11

Interionic distance	*Radius* Å
Mn—O: 2·20	0·80
Mn—F: 2·12	0·79
Fe—O: 2·15	0·75
Fe—O: 2·14	0·74
Fe—F: 2·06	0·73
Co—O: 2·12	0·72
Co—F: 2·04	0·72
Ni—O: 2·09	0·69
Ni—F: 2·02	0·69

Agreement between radii derived from oxides and from fluorides is excellent.

For these ions, polarizing power increases in the order, Mn, Fe, Co, Ni and it is not known to what extent Ni^{2+} in particular might cause shrinkage of O^{2-} or F^-; it does not appear to be marked.

Radii of Cr^{3+} (0·63 Å), Fe^{3+} (0·64 Å) and Rh^{3+} (0·68 Å) are based in part on interionic Cr—O, Fe—O, Rh—O and Ga—O measurements by Zachariasen (Goldschmidt [1], p. 29) using a radius of 0·62 Å for Ga^{3+} (Table 1) as calibration, and in part, on the approximate method described below (see radii of Ge^{2+}, Cu^{2+}, etc.). Apparent decrease in the radius of O^{2+} is about 0·05–0·1 Å in these R_2O_3 crystals.

(7) Approximate radii of V^{4+}, Mn^{4+}, Nb^{4+}, Mo^{4+}, Ru^{4+}, Te^{4+}, W^{4+}, Os^{4+} and Ir^{4+}

Oxides of these elements assume the rutile structure. Because these ions invariably cause a shrinkage in O^{2-} which is difficult to assess accurately, their radii cannot be determined accurately. Use may, however, be made of the data in Table 12 which compares radii of Ti^{4+}, Pb^{4+} and Sn^{4+} from Table 1 with those obtained from interionic distance measurements.

A significant shrinkage (0·05–0·12 Å) is evident and a similar shrinkage is to be expected in rutile structures (RO_2) containing V^{4+}, Mn^{4+}, Nb^{4+}, Mo^{4+}, Ru^{4+}, Te^{4+}, W^{4+}, Os^{4+} and Ir^{4+}. Table 13 shows radii of these ions obtained by subtracting 1·30 Å for O^{2-} (allowance of 0·1 Å for shrinkage) from interionic distance measurements. Because GOLDSCHMIDT [1] used an O^{2-} radius of 1·32 Å, many radii in Table 13 are similar to his values.

Radii marked with an asterisk have been used in compiling the final set given in Table 16. For Mn^{4+}, Nb^{4+} and Te^{4+}, values obtained by the method described below are recommended. Thus the radius of Nb^{4+} given above (0·71 Å) appears a little low when compared with that of $Nb^{5+} = 0{\cdot}69$ Å (Table 1) and the value (0·74 Å) given in Table 16 is recommended.

Table 12

Interionic distance Å	*Radius* Å ($O^{2-} = 1{\cdot}40$)	*Radius* Å *(Table 1)*	*Apparent* O^{2-} *shrinkage* Å
Ti—O : 1·96	0·56	0·68	0·12
Pb—O : 2·16	0·76	0·84	0·08
Sn—O : 2·06	0·66	0·71	0·05

Table 13. Radii of some 4⁺ ions (rutile structures)

Interionic distance Å	*Radius* Å
V—O : 1·93	0·63*
Mn—O : 1·84	0·54
Nb—O : 2·01	0·71
Mo—O : 2·00	0·70*
Ru—O : 1·97	0·67*
(Te—O : 2·21	0·91)
W—O : 2·00	0·70*
Os—O : 1·99	0·69*
Ir—O : 1·98	0·68*

Like comments apply to Mn^{4+}. In the TeO_2 crystal there is an anomalous axial ratio and it is difficult to give a measured radius of Te^{4+} with confidence.

(8) Approximate radii obtained with the aid of ionization potentials.

The radii of several ions which are not members of normal isoelectronic sequences cannot be determined satisfactorily from interionic distance measurements: either structurally ionic crystals are not available, (for example, compounds containing Pd^{2+} and Au^{3+} and other ions which have extremely high polarizing powers) or, if they are, it might not be possible to make accurate allowance for decrease in the apparent size of O^{2-} (radius of Nb^{4+} for example).

The radius of an ion may be determined approximately by utilizing the change of radius with ionization potential for ions of an element in their different valence states.

Two assumptions will be made, both of which are approximate:

(i) that the relationship,

$$r = \frac{K}{I^n}$$

holds for different ions of one element, and,

(ii) that the exponent n, is approximately the same for all elements. K is a separate constant for each element.

The pairs of ions, Mn^{2+} and Mn^{7+}, and Tl^{+} and Tl^{3+}, whose radii are accurately known, serve as calibration ions, and using the data in Table 14, n may be determined graphically using log-log co-ordinates. n is the slope of a straight line drawn through each pair of calibration ions and is found to equal 3·5 for both pairs.

For calculating the radius of an unknown, for example Ge^{2+}, a reference ion, Ge^{4+} ($r = 0{\cdot}53$ Å, $I = 45{\cdot}7$ v) is used to determine K. Substitution of $I = 15{\cdot}9$ v for Ge^{2+} gives the approximate radius of 0·73 Å for this ion. This determination could of course also be carried out graphically on log-log co-ordinates.

Ionic radii derived in this way are given in Table 15.

Those radii which are most approximate have been bracketed; values should, however, usually be within about 0·1 Å of the correct value.

Table 14

Ion	*r* Å	*I* *volts*
Mn^{2+}	0·80	15·6
Mn^{7+}	0·46	122
Tl^{+}	1·47	6·1
Tl^{3+}	0·95	29·8

Table 15. Some approximate radii obtained with the aid of ionization potentials

Ion	*Radius* Å	*Ion*	*Radius* Å
I^{5+}	0·62	Br^{5+}	0·47
Ge^{2+}	0·73	S^{4+}	0·37
Cu^{2+}	0·72	Se^{4+}	0·50
As^{3+}	0·58	Te^{4+}	(0·70)
Sb^{3+}	0·76	N^{3+}	0·16
Bi^{3+}	0·96	P^{3+}	0·44
V^{2+}	(0·88)	Mn^{3+}	(0·66)
V^{3+}	0·74	Mn^{4+}	(0·60)
V^{4+}	0·63	Pt^{2+}	(0·80)
Ti^{3+}	0·76	Pd^{2+}	(0·80)
Ce^{4+}	0·93	Au^{3+}	(0·85)
Nb^{4+}	0·74	Re^{4+}	(0·72)
Cl^{5+}	0·34		

Ionization potentials for Mn^{3+}, Mn^{4+} and Au^{3+} were not available and approximate values were obtained either by extrapolation or interpolation.

All radii discussed here are gathered and arranged alphabetically in Table 16. As in other sets, these radii are for ions in 6-fold co-ordination.

Table 16. Ionic radii of cations (6 fold co-ordination)

Ac^{3+}	1·18	Cd^{2+}	0·97	Ga^{3+}	0·62	Mo^{4+}	0·70
Ag^{+}	1·26	Ce^{3+}	1·07	Gd^{3+}	0·97	Mo^{6+}	0·62
Ag^{2+}	0·89	Ce^{4+}	0·94	Ge^{2+}	0·73	N^{3+}	0·16
Al^{3+}	0·51	Cl^{5+}	0·34	Ge^{4+}	0·53	N^{5+}	0·13
Am^{3+}	1·07	Cl^{7+}	0·27	Hf^{4+}	0·78	Na^{+}	0·97
Am^{4+}	0·92	Co^{2+}	0·72	Hg^{2}	1·10	Nb^{4+}	0·74
As^{3+}	0·58	Co^{3+}	0·63	Ho^{3+}	0·91	Nb^{5+}	0·69
As^{5+}	0·46	Cr^{3+}	0·63	I^{5+}	0·62	Nd^{3+}	1·04
At^{7+}	0·62	Cr^{6+}	0·52	I^{7+}	0·50	Ni^{2+}	0·69
Au^{+}	1·37	Cs^{+}	1·67	In^{3+}	0·81	Np^{3+}	1·10
Au^{3+}	0·85	Cu^{+}	0·96	Ir^{4+}	0·68	Np^{4+}	0·95
B^{3+}	0·23	Cu^{2+}	0·72	K^{+}	1·33	Np^{7+}	0·71
Ba^{2+}	1·34	Dy^{3+}	0·92	La^{3+}	1·14	O^{6+}	0·10
Be^{2+}	0·35	Er^{3+}	0·89	Li^{+}	0·68	Os^{6+}	0·69
Bi^{3+}	0·96	Eu^{3+}	0·98	Lu^{3+}	0·85	P^{3+}	0·44
Bi^{5+}	0·74	F^{7+}	0·08	Mg^{2+}	0·66	P^{5+}	0·35
Br^{5+}	0·47	Fe^{2+}	0·74	Mn^{2+}	0·80	Pa^{3+}	1·13
Br^{7+}	0·39	Fe^{3+}	0·64	Mn^{3+}	0·66	Pa^{4+}	0·98
C^{4+}	0·16	Fr^{+}	1·80	Mn^{4+}	0·60	Pa^{5+}	0·89
Ca^{2+}	0·99			Mn^{7+}	0·46		

Table 16. (Continued)

Pb^{2+}	1·20	Re^{4+}	0·72	Sn^{2+}	0·93	Tm^{3+}	0·87
Pb^{4+}	0·84	Re^{7+}	0·56	Sn^{4+}	0·71	U^{4+}	0·97
Pd^{2+}	0·80	Rh^{3+}	0·68	Sr^{2+}	1·12	U^{6+}	0·80
Pd^{4+}	0·65	Ru^{4+}	0·67	Ta^{5+}	0·68	V^{2+}	0·88
Pm^{3+}	1·06	S^{4+}	0·37	Tb^{3+}	0·93	V^{3+}	0·74
Po^{6+}	0·67	S^{6+}	0·30	Tb^{4+}	0·81	V^{4+}	0·63
Pr^{3+}	1·06	Sb^{3+}	0·76	Tc^{7+}	0·56	V^{5+}	0·59
Pr^{4+}	0·92	Sb^{5+}	0·62	Te^{4+}	0·70	W^{4+}	0·70
Pt^{2+}	0·80	Sc^{3+}	0·81	Te^{6+}	0·56	W^{6+}	0·62
Pt^{4+}	0·65	Se^{4+}	0·50	Th^{4+}	1·02	Y^{3+}	0·92
Pu^{3+}	1·08	Se^{6+}	0·42	Ti^{3+}	0·76	Yb^{3+}	0·86
Pu^{4+}	0·93	Si^{4+}	0·42	Ti^{4+}	0·68	Zn^{2+}	0·74
Ra^{2+}	1·43	Sm^{3+}	1·00	Tl^{+}	1·47	Zr^{4+}	0·79
Rb^{+}	1·47			Tl^{3+}	0·95		

References

[1] Goldschmidt, V. M. with Barth, T., Lunde, G. and Zachariasen, W.; Geochemische Verteilungsgesetze der Elemente. VII. Skr. Norske Vid.-Akad. Oslo. 1, Mat.-Nat. Kl. No. 2, 1926. [2] Pauling, L.; The sizes of ions and the structure of ionic crystals. J. Amer. Chem. Soc. 1927 **49** 763. [3] Zachariasen, W. H.; A set of empirical crystal radii for ions with inert gas configuration. Z. Krist. 1931 **80** 137. [4] Wyckoff, R. W. G.; Crystal Structures. Interscience Publishers Inc., New York, 1951. [5] Pauling, L.; The nature of the chemical bond. 2d. Ed. 1945. Cornell University Press. [6] Wyckoff, R. W. G.; The structure of crystals. The Chemical Catalog Co. Inc., 1924. [7] Wasastjerna, J.; On the radii of ions. Soc. Sci. Fenn., Comm. Phys. Math. 1 1923 **38** 22. [8] Evans, R. C.; An introduction to crystal chemistry. Cambridge University Press, 1946. [9] Pauling, L. and Sherman, J.; Screening constants for many-electron atoms. The calculation and interpretation of x-ray term values, and the calculation of atomic scattering factors. Z. Krist. 1932 **81** 1. [10] Fajans, K. and Joos, G.; Molrefraktion von Ionen und Molekülen im Lichte der Atomstruktur. Z. Phys. 1924 **23** 1. [11] Fajans, K.; II. Die Eigenschaften salzartiger Verbindungen und Atombau. Z. Krist. 1925 **61** 18. [12] Herzberg, G.; Atomic spectra and atomic structure. Dover Publications, New York, 1945. [13] Lisitzin, E.; Über die Ionisierungsspannungen der Elemente. Soc. Sci. Fenn., Comm. Phys.-Math., X, No. 1, 1938. [14] Harrison, G. R., Lord, R. C. and Loofbourow, J. R.; Practical Spectroscopy. Prentice Hall, New York, 1948. [15] Hevesey, G. von; Über Gesetzmäßigkeiten innerhalb der seltenen Erden und der Titangruppe. Z. anorg. chem., 1925 **147** 217. [16] Goldschmidt, V. M.; Geochemische Verteilungsgesetze der Elemente. Skr. Norske. Vid.-Akad. Oslo 1. Mat.-Nat. Kl. No. 7 1925. [17] Bommer, H.; Die Gitterkonstanten der C-Formen der Oxyde der seltenen Erdmetalle. Z. anorg. Chem. 1939 **241** 273. [18] Schulze, G. E. R.; The crystal structure of RaF_2. Z. Phys. Chem. (B) 1936 **32** 430. [19] Löhberg, K.; Über die C-Modifikation der Sesquioxyde von Nd und La. Z. phys. Chem. (B) 1935 **28** 402. [20] Zachariasen, W. H.; Norske Vid. Akad. Oslo, 1. Mat.-Nat. Kl. 4, 1928. [21] Zachariasen, W.H.; Crystal radii of the heavy elements. Phys. Rev. 1948 **73** 1104.

Geochimica et Cosmochimica Acta, 1952, Vol. 2, pp. 170 to 184. Pergamon Press Ltd., London

Behaviour of the trace elements in a front of metasomatic-metamorphism in the Dalradian of Co. Donegal

Riad A. Higazy

Farouk I University, Alexandria, Egypt*

(Received 24 October 1951)

ABSTRACT

The epidiorite and quartzite of the Malin Head district, (Ireland) are considered by Holmes and Reynolds [7] to be metasomatically transformed into skarn-rocks and mica-schist respectively. The trace element contents of these rocks were investigated using semi-quantitative methods in order to study the behaviour of the different trace elements during the metasomatic changes which have taken place. The elements which have been determined are Rb, Ba, Ag and Pb; Sr, Y and La; Li, Cr, Ni, Co, V, Cu, Sc, Sn and Mo; Ga; Zr, Be, Tl, Ge and In. The trace elements follow the major elements for which they can substitute in favourable crystal lattices, the substitution being in accord with Goldschmidts rules. Rb, Ba and probably Pb and Ag follow and substitute for K; Sr and Y for Ca and probably K; Li, Cr, Ni, Co, V, Cu, Sc, Sn and Mo for Mg, Fe^2 and Fe^3; and Ga for Al.

Introduction

In their study of the White Cow epidiorite sills of the Malin Head district, Inishowen, Co. Donegal, Eire, in the most northerly part of Ireland, Holmes and Reynolds [7] have established the following sequence of rock types:

$$\text{epidiorite} \rightarrow \text{biotite-epidiorite} \rightarrow \text{biotite-skarn} \begin{cases} \nearrow \text{lepidomelane-skarn} \\ \searrow \text{chlorite-skarn} \end{cases}$$

They have also discovered and investigated the following transition:

$$\text{quartzite} \rightarrow \text{mica-schist.}$$

The quartzite underlies the main White Cow sill and separates the latter from an underlying thinner epidiorite sill. For the general geology of the district and a geological map see Holmes and Reynolds [7] (p. 28 and Fig. 3, p. 29).

From field evidence and microscopic examination a metasomatic derivation of the skarn rocks from the epidiorite, and of the mica-schist from the quartzite is inferred. Differential atomic migration of the various elements and reorganization of the constituents of the country-rocks in the solid state are thought to be responsible for the metasomatic changes that have taken place. Gaseous transfer is considered inadequate, since a gas phase is most likely to be acidic, whereas in the metasomatic changes under consideration introduction of alkaline materials were dominant. Moreover, hydrothermal solutions could not readily account for the transformations, since cracks, fissures and other passageways which could assist circulating solutions in penetrating rocks such as quartzite are lacking.

The metasomatic changes mentioned above are considered to be complementary to granite formation. The skarn-rocks and the mica-schist are regarded as represen-

* On study leave at the Grant Institute of Geology, University of Edinburgh, Scotland.

tatives of a basic front, possibly to be correlated with the development of syntectonic migmatites elsewhere.

The chemical changes involved in the transformation processes and responsible for the change from epidiorite to skarn-rocks have been, on the whole, increase of MgO, (total FeO + MgO), K_2O, H_2O, P_2O_5 and MnO and decrease of Al_2O_3, CaO and Na_2O.

The transformation of quartzite to mica-schist seems to have resulted from similar changes to that found for development of the skarn-rocks from epidiorite; thus there seems to have been an increase of Al_2O_3, total FeO, MgO, K_2O, H_2O, TiO_2, P_2O_5 and MnO and decrease of SiO_2, $CaCO_3$, CaO and Na_2O.

The present study is an investigation of the behaviour of the trace elements during this metasomatic-metamorphism. Using spectrographic methods, the author has analysed the following rocks of the Malin Head district for their trace elements: epidiorite (No. 94), biotite-epidiorite (No. 350), biotite-skarn (No. 92), lepidomelane-skarn (No. 381) and chlorite-skarn (No. 353); quartzite (No. 394) and mica-schist (No. 395). Petrographic description and chemical analyses of these rocks are given by Holmes and Reynolds and their exact location is illustrated ([7], Fig. 4, p. 30 and Fig. 6, p. 34).

Table 1

Element *	*Wave length in Å*	*Sensitivity in ppm*
Rb	7800·2	1
Li	6707·8	1
Ba	4934·1	5
Sr	4607·3	5
La	4333·7	30
Cr	4254·3	1
Sc	3911·9	10
Co	3483·5	2
Ni	3414·8	2
Zr	3391·9	10
Y	3327·9	30
Ag	3280·7	1
Cu	3247·6	3
V	3185·4	5
Mo	3170·3	1
Be	3131·7	5
In	3039·4	10
Ga	2943·6	1
Sn	2840·0	5
Pb	2833·1	10
Tl	2767·9	30
Ge	2651·6	10

* For ionic radii see Table 4.

Analytical Methods and the Data Obtained

Portions of the powders used for the chemical analyses were kindly provided by Prof. A. Holmes and Dr. D. L. Reynolds. The spectrographic analyses were made at the Macaulay Institute for Soil Research at Aberdeen.

The semi-quantitative analytical method adopted in this study has already been described in detail by Mitchell [9].

The determined elements, the respective wave lengths of their diagnostic lines and the sensitivity of each element are listed in Table 1.

The percentages of the major oxides determined chemically, quoted from Holmes and Reynolds [7], as well as those of the different trace elements are recorded in Table 2. The rock formula (based on a unit cell of 160 oxygen atoms as introduced by Barth [2] for metasomatic processes) of each of the analysed rocks was calculated with the results listed in Table 3. Figs. 1–5 show the significant gains and losses of the various elements involved at each stage of the transformation processes.

Alterations of the Epidiorite

(a) *Alteration of epidiorite A to biotite-epidiorite B*

The unmodified epidiorite of the sill (No. 94) is formed of narrow alternating bands which differ in colour. The relatively dark bands are rich in hastingsite and contain some iron-ore, sphene, a little epidote and occasional biotite. The relatively light

Table 2. Chemical and spectrographic composition in weight per cent

Oxide	*A*	*B*	*C*	*D*	*E*	*F*	*G*
SiO_2	47·32	48·34	45·65	48·13	44·98	72·06	65·36
Al_2O_3	17·39	15·49	15·56	14·76	14·44	10·92	15·68
Fe_2O_3	2·36	2·14	2·55	7·34	3·02	0·04	1·49
FeO	10·91	10·60	11·21	6·38	10·98	1·40	4·32
MgO	4·78	5·56	5·01	6·61	6·08	0·31	1·79
CaO	10·08	9·42	7·94	6·18	8·24	6·02	0·83
Na_2O	2·73	1·98	0·01	0·43	0·16	2·93	2·16
K_2O	0·54	1·36	4·77	3·59	1·23	1·16	4·54
H_2O^+	0·96	1·54	2·35	2·82	5·19	0·84	2·32
CO_2	tr.	none	2·02	none	1·74	3·98	none
TiO_2	2·68	2·48	2·30	2·58	2·92	0·08	0·86
P_2O_5	tr.	0·32	0·30	0·22	0·29	none	0·18
MnO	0·20	0·34	0·23	0·32	0·35	0·07	0·21
Rb_2O	0·0005	0·006	0·066	0·08	0·009	0·004	0·076
Li_2O	0·002	0·005	0·017	0·01	0·02	0·0006	0·004
BaO	0·01	0·03	0·1	0·08	0·03	0·1	0·33
SrO	0·12	0·11	0·165	0·077	0·03	0·21	0·06
La_2O_3	*	*	*	*	*	0·005	0·006
Cr_2O_3	0·003	0·01	0·007	0·033	0·009	0·0003	0·01
Sc_2O_3	*	*	0·003 ?	*	*	*	0·001
CoO	0·009	0·01	0·01	0·01	0·006	0·0001	0·003
NiO	0·008	0·01	0·008	0·01	0·01	0·0004	0·006
ZrO_2	0·027	0·027	0·022	0·014	0·014	0·032	0·135
Y_2O_3	0·009	0·008	0·01	0·01	0·009	0·006	0·01
Ag_2O	<0·0001	0·0001	0·0004	<0·0001	* ?	0·0007	0·0002
CuO	0·03	0·04	0·01	0·03	0·04	0·08	0·06
V_2O_3	0·05	0·047	0·05	0·045	0·045	0·01	0·015
MoO_2	<0·0001	0·0003	*	*	<0·0001	*	*
BeO	*	*	*	*	*	<0·001	0·002
In_2O_3	*	*	*	*	*	*	*
Ga_2O_3	0·005	0·005	0·005	0·005	0·003	0·003	0·005
SnO_2	*	0·01	*	0·0006	0·001	0·01 ?	0·004
PbO	<0·001	0·005	<0·001	0·002	0·001	0·01	0·004
Tl_2O	*	*	*	*	*	*	*
GeO_2	*	*	*	*	*	*	*

A Epidiorite (No. 94), *B* Biotite-epidiorite (No. 350), *C* Biotite-skarn (No. 92), *D* Lepidomelane-skarn (No. 381), *E* Chlorite-skarn (No. 353); *F* Quartzite (No. 394) and *G* Mica-schist (No. 395).

Chemical analyses in Holmes and Reynolds [7], include:

	H_2O^-	BaO	NiO	*Total*	*Analyst*
A	0·05	0·01	—	100·01	Agnes Gibbs
B	0·16	—	—	99·73	W. H. Herdsman
C	0·10	0·02	tr.	100·02	Agnes Gibbs
D	0·39	—	—	99·75	W. H. Herdsman
E	0·18	—	—	99·80	W. H. Herdsman
F	0·26	—	—	100·07	W. H. Herdsman
G	0·34	—	—	100·08	W. H. Herdsman

Spectrographic analyst: R. A. Higazy.

* = Element if present is in amount below the corresponding limit of sensitivity given in Table 1.

Error is of the order of 25–30% over the range of approximately 10 to 300 ppm. If the element is over 1000 ppm errors of 50% are possible.

Table 3. Rock formulae of the analysed rocks

Element	*A*	*B*	*C*	*D*	*E*	*F*	*G*
Si	45·96	46·45	43·50	45·75	41·20	61·00	57·50
Al	19·80	17·40	17·40	16·50	15·50	10·90	16·22
Fe^3	1·72	1·54	1·82	5·25	2·08	0·03	1·47
Fe^2	8·87	8·44	8·92	5·06	8·42	0·99	3·17
Mg	6·90	7·96	7·10	9·36	8·32	0·40	2·35
Ca	10·40	9·66	8·10	6·30	8·12	5·47	0·78
Na	5·14	3·66	0·02	0·78	0·28	4·82	3·66
K	0·67	1·66	5·80	4·36	1·44	1·24	5·10
H	6·20	9·82	14·90	17·90	31·60	4·72	13·60
C	tr.	none	2·62	none	2·16	4·61	none
Ti	1·95	1·78	1·64	1·83	2·02	0·05	0·56
P	tr.	0·26	0·24	0·18	0·22	none	0·14
Mn	0·16	0·27	0·18	0·26	0·27	0·05	0·16
Rb	0·0003	0·004	0·04	0·048	0·005	0 002	0·04
Li	0·008	0·02	0·06	0·04	0·07	0·002	0·016
Ba	0·004	0·012	0·037	0·03	0·01	0·03	0·1
Sr	0·066	0·06	0·09	0·04	0·015	0·1	0·03
La	*	*	*	*	*	0·0015	0·002
Cr	0·002	0·008	0·005	0·024	0·006	0·0002	0·009
Sc	*	*	0·002 ?	*	*	*	0·001
Co	0·007	0·0087	0·0086	0·008	0·005	0·00007	0·002
Ni	0·006	0·008	0·006	0·009	0·007	0·0002	0·004
Zr	0·01	0·01	0·01	0·006	0·007	0·01	0·06
Y	0·005	0·004	0·0054	0·0058	0·0046	0·003	0·006
Ag	0·00004	0·00002	0·0002	0·00004	*	0·0003	0·00004
Cu	0·02	0·03	0·009	0·02	0·03	0·05	0·04
V	0·037	0·036	0·039	0·035	0·033	0·007	0·01
Mo	0·00004	0·0001	*	*	0·00005	*	*
Be	*	*	*	*	*	0·003	0·004
In	*	*	*	*	*	*	*
Ga	0·0029	0·0028	0·0028	0·003	0·002	0·002	0·003
Sn	*	0·005	*	0·0002	0·0005	0·004	0·001
Pb	0·0003	0·001	0·0003	0·0004	0·0003	0·003	0·001
Tl	*	*	*	*	*	*	*
Ge	*	*	*	*	*	*	*

A–G as in Table 2.

coloured bands are composed of feldspar, small crystals of epidote and occasional garnet ([7] p. 31). The biotite-epidiorite (No. 350) is composed of hastingsite, quartz, oligoclase with abundant associated sericite, finely granular epidote, relatively large flakes of biotite, and a little sphene, black iron-ore and pyrite. The biotite which is partially altered to ripidolite, replaces the original constituents of the epidiorite.

The mineralogical changes are, therefore, an increase of biotite and quartz at the expense, principally, of amphibole and sodic plagioclase. The chemical changes which have been determined by analysis correspond fairly closely to the changes which would be anticipated from the observed mineralogical changes.

Reference to Table 3 and Fig. 1 shows that the most significant gains in the formation of the biotite-epidiorite are: Mg 1·06 and K 0·99; and that the losses are: Al 2·40, Na 1·48 and lesser amounts of Ca 0·74, Fe^2 0·43 and Fe^3 0·18.

The minor elements which were added to the epidiorite are P and Mn, while the trace elements gained are Cr, Ni, Co, Li, Cu, Mo, Sn, Rb, Ba and Pb. One minor element, Ti, was subtracted, and the trace elements lost are Sr, Y, V, Ga and Ag.

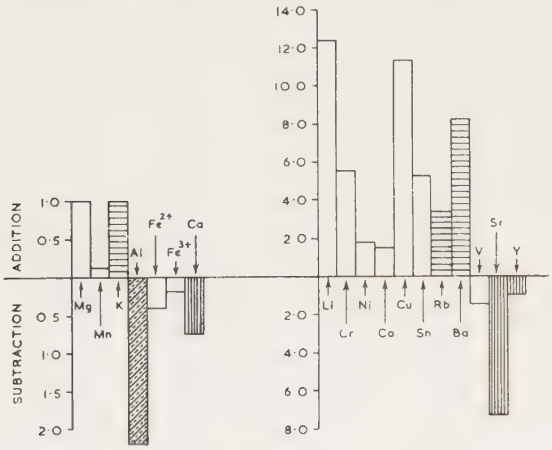

Fig.1. Addition and subtraction (per rock "unit cell") of major and trace elements during the transformation of epidiorite (*A*) to biotite-epidiorite (*B*). The amounts in the case of the trace elements are multiplied by 1000.

There are still six elements, namely, La, Tl, Sc, Ge, Be and In, which if present in the epidiorite and/or biotite-epidiorite, are in amounts below the limits of sensitivity given in Table 1. Any change in these elements is, therefore, undetectable.

Table 4 shows for each of the major rock forming elements, namely, Si^{4+}, Al^{3+}, Fe^{2+}, Fe^{3+}, Mg^{2+}, Ca^{2+}, Na^{+} and K^{+} which of the minor and trace elements are believed to substitute for it, under favourable conditions of temperature and pressure and in the appropriate crystal lattices. Substitution may be by camouflage, capture or admission depending on the electrostatic charges and the radii of the elements concerned ([4], [5] and [6]).

It is significant that in the transformation process under review—epidiorite to biotite-epidiorite—each trace element, whether added or subtracted, follows quite

*Table 4. Possible substitutions for the common rock-forming elements**

Major element	Mg^{2+}	Na^{+}	Fe^{2+}	Fe^{3+}	K^{+}	Ca^{2+}	Al^{3+}	Si^{4+}
Substituting elements	Fe^{3+}	Mg	Mg	Al	Ag^{+}	Na	Fe^{3+}	Al
	Cr^{3+}	Fe^{2+}	Co^{2+}	Cr^{3+}	La^{3+}	In^{3+}	Cr^{3+}	Be^{2+}
	Mo^{4+}	Co^{2+}	Ca	Ga^{3+}	Pb^{2+}	Mn^{2+}	Ga^{3+}	P^{5+}
	Li^{+}	Cu^{2+}	Li^{+}	V^{3+}	Sr^{2+}	Ag^{+}	V^{3+}	Ge^{4+}
	Ni^{2+}	Zr^{4+}	Sc^{3+}	Ti^{4+}	Ba^{2+}	La^{3+}	Ti^{4+}	
	Ti^{4+}	In^{3+}	Ni^{2+}	Mg	Rb^{+}	Sr^{2+}	Mo^{4+}	
	V^{3+}	Li^{+}	Mo^{4+}	Li^{+}	Tl^{+}			
	Sn^{4+}	Ni^{2+}	Sn^{4+}	Ni^{2+}				
	Fe^{2+}	Mn^{2+}	Na	Mo^{4+}				
	Co^{2+}	Sc^{3+}	Zr^{4+}	Sn^{4+}				
	Cu^{2+}	Sn^{4+}	In^{3+}					
	Zr^{4+}	Ca	Mn^{2+}					
	In^{3+}	Ag^{+}						
	Mn^{2+}	Y^{3+}						
	Sc^{3+}							

* Ionic radii in KX for 6-fold-coordination taken from Rankama, K. and Sahama, Th. G. "Geochemistry," Univ. Chicago Press 1950, appendix 3, pp. 794–795 are:

Mg^{2+} 0·78, Na^{+} 0·98, Fe^{2+} 0·83, Fe^{2+} 0·67, K^{+} 1·33, Ca^{2+} 1·06, Al^{3+} 0·57, Si^{4+} 0·39, Ag^{+} 1·13, Ba^{2+} 1·43, Be^{2+} 0·34, Co^{2+} 0·82, Cr^{3+} 0·64, Cu^{2+} 0·83, Ga^{3+} 0·62, Ge^{4+} 0·44, In^{3+} 0·92, La^{3+} 1·22, Li^{+} 0·78, Mn^{2+} 0·91, Mo^{4+} 0·68, Ni^{2+} 0·78, P^{5+} 0·35, Pb^{2+} 1·32, Rb^{+} 1·49, Sc^{3+} 0·83, Sn^{4+} 0·74, Sr^{2+} 1·27, Ti^{4+} 0·64, Tl^{+} 1·49, V^{3+} 0·65, Y^{3+} 1·06, and Zr^{4+} 0·87.

closely the major element with which it can form a substituting pair. Li, Cr, Ni, Co and Cu follow Mg; Rb, Ba and Pb follow K; and Sr follows Ca.

Ferrous and ferric iron were both subtracted from the epidiorite. Neither Co nor Cr was subtracted though they have approximately similar ionic radii with Fe^2 and Fe^3 respectively. However the gain in Mg is much greater than the loss in total iron. Co and Cr which can proxy for Mg, Fe^2 and Fe^3 followed Mg in this case. V on the other hand, was subtracted, as was ferric iron. V^3 has an ionic radius 0·65 Å very nearly the same as that of Fe^3 0·67 Å. Ti, having an ionic radius of 0·64 Å, was also subtracted, thus behaving like Fe^3.

The gain in Mg is 1·06, while the total loss of both Fe^2 and Fe^3 is only 0·61. The trace elements which can substitute for Mg, Fe^2 and Fe^3, as shown in Table 4, are Li, Cr, Co, Ni, Cu, Sn, Mo and V. Amongst these elements, V was subtracted, whereas the others were added. The total of the added ions (0·036) exceeds that of the subtracted ions (0·001), as in the case of their respectibe interchangeable major elements.

Rb and Ba were added, clearly following K. Sr can substitute for both Ca and K. But in this case it followed Ca. It may be surmised that Ba and Rb, having apparently satisfied what the potassium mineral lattices could accommodate, left Sr to follow Ca. Just as the added amount of K exceeds that of the subtracted Ca, so the added Rb and Ba (0·01) is also higher than the subtracted Sr, Y and Ag (0·007). Y is known to substitute for Ca while Ag can replace both K and Ca.

Ga following Al was subtracted. It is not clear at this stage which trace elements follow Na. It can be said that the loss in Na accounts for the relative impoverishment of the biotite-epidiorite in soda-plagioclase. It seems that the substitution in the feldspar lattice takes place mainly with respect to Ca and K. The ions which can substitute for Na are Co, Cu, Ni, Li and Sc. The feldspar lattice is not favourable for these ions, since they have relatively low coordination numbers. Moreover, they have high activation energy values [13], and therefore, can preferentially substitute in minerals formed at higher temperatures than those appropriate to the crystallization of sodic plagioclase. In soda-amphiboles and soda-pyroxenes, for example, Co, Cu, Ni, Li and Sc can replace Mg and/or Fe, while their substitution for Na cannot be justified. The same trace elements are commonly found in the olivines. Soda-olivines, however, are not known as natural minerals and so far have not been synthesized. It would appear that Na, which can exist in the silicon-oxygen chain structures of amphiboles and pyroxenes, cannot take part in the tetrahedral structure of olivines which, moreover, form at temperatures apparently too high for Na to play a role in their composition.

Table 5 gives the ratio of each of the trace elements to its interchangeable major element. The ratio Ga/Al, Ni/Mg and Co/Fe^2 are approximately the same in the epidiorite (amphibole-rich rock) and the biotite-epidiorite (biotite-rich rock). Ga, Ni and Co seem to enter into the amphibole and the biotite lattices with about equal ease. On the other hand, the biotite-rich rock B, has higher Li/Mg, Ba/K and (Ba + Rb)/K ratios and a lower Sr/K ratio with comparison to the amphibole-rich rock. Nockolds has mentioned similar findings (in Nockolds and Mitchell [10] pp. 551–552) regarding the hornblendes and biotites occurring in certain Caledonian plutonic rocks which are mainly of granodioritic composition. He considered such characteristic tendencies in the ratios under discussion as an indication that

Table 5. Ratios of trace to major elements in the analysed rocks

*Ratio**	*A*	*B*	*C*	*D*	*E*	*F*	*G*
Ga/Al	0·39	0·42	0·42	0·51	0·33	0·43	0·48
Ni/Mg	2·08	2·39	2·03	2·26	2·04	1·60	4·12
Co/Mg	2·43	2·69	2·81	2·01	1·37	0·53	2·32
Li/Mg	0·35	0·75	2·50	1·25	2·45	1·60	1·85
Co/Fe^{2+}	0·83	1·09	1·03	1·61	0·59	0·09	0·74
Cr/Fe^{3+}	1·21	4·68	2·80	4·38	2·85	7·15	8·62
Sr/Ca	14·00	13·40	24·62	14·75	4·25	41·70	84·50
Sr/(Ca + K)	13·15	11·41	14·50	8·80	3·62	34·20	10·90
Ba/K	22·20	26·60	22·70	25·20	27·40	93·50	79·80
Ba/(K + Ca)	1·32	3·81	9·39	10·12	4·05	17·10	67·00
Rb/K	1·11	4·87	15·15	26·80	8·30	4·14	18·50
Sr/K	222·00	79·60	35·40	21·80	24·40	187·00	13·25
(Rb + Ba)/K	23·31	31·47	37·85	52·00	35·70	97·64	98·30
(Sr + Rb + Ba)/K	245·31	111·07	73·25	73·80	60·10	284·64	111·55

A–G as in Table 2.

* Ratios are expressed as multiplied by 1000 in each case.

hornblende crystallized from magmatic sources earlier than biotite. Supposing for the sake of argument that Nockolds is right in ascribing a magmatic origin to these minerals, one would therefore be led to the belief that the fundamental principles of replacement of the major elements by the trace elements remain essentially the same, whether the mineral concerned is formed from magmatic melts, migrating atoms or even granitizing solutions. The same mineral, so far as our knowledge goes, has the same crystal lattice and reveals essentially the same geochemical relationships in every case.

The paragenesis of minerals on the basis of the behaviour of the trace elements would not then provide conclusive evidence for a magmatic derivation. This inference is independent of the fact that the order of crystallization in magmatic rocks can rarely be judged with adequate certainty. The minerals are known to overlap during their development.

Buerger and Washkin [3] show that during metamorphism, a mineral will recrystallize only when it is heated above a certain critical temperature which varies with the mineral and is characteristic of it. Each of the known facies of the metamorphic rocks forms under specific conditions of temperature and pressure. Metasomatic products also depend on the temperature prevailing during the replacement. The effect of temperature on the substitution of the trace elements for their interchangeable major elements would be the same in all the different crystalline-rock formation processes. A given trace element, whether present in the magmatic melt, in the country rocks or in the replacing materials, appears to enter into any favourable mineral lattice, following the same geochemical rules in every case.

Ahrens [1] has established that thallium and rubidium are enriched in replacement microclines. This enrichment accords well with Goldschmidts rules for substitution. Jaffe [8] studied the trace elements of garnets from pegmatites and from metamorphic rocks, namely, schists and tactites. Again, he finds that Goldschmidts concepts of substitution of the trace elements hold true in every case. The pegmatite garnets are manganese rich, where Y (ionic radius 0·83 Å) proxies

for Mn (0·91 Å). The garnets of the schist are rich in magnesium and iron where Sc (0·83 Å) proxies for either Mg (0·78 Å) or Fe^2 (0·83 Å). The garnets of the tactites are calcium rich where Sr (1·27 Å) proxies for Ca (1·06 Å). These replacements are essentially similar to those here shown to characterise the metasomatic transformation of epidiorite to biotite-epidiorite.

(b) *Alteration of biotite-epidiorite B to biotite-skarn C*

Gradation between biotite-epidiorite and skarn is found in place ([7] p. 37). The significant mineralogical change in this transformation is the great increase of biotite at the expense of hastingsite.

Table 3 and Fig. 2 indicate that the biotite-epidiorite gained K 4·14, Fe^2 0·48 and Fe^3 0·34, and lost the following: Na 3·58, Ca 1·56 and Mg 0·86. The trace elements which were added are Li, V and Sc; Rb, Ba, Sr, Y and Ag. The subtracted minor and trace elements are respectively, Ti and Mn, and Cr, Co, Ni, Cu, Sn, Mo; and Pb.

It is noticeable that V and Sc followed iron. It is quite likely that V replaced Fr^3, and Sc substituted for Fe^2 with other appropriate substitutions taking place, mainly in the biotite lattice, to balance the electrostatic charge. It might be recalled that Li was added in the replacement of hastingsite by biotite to form the biotite-epidiorite. The same happened when more biotite replaced hastingsite to give rise to the biotite-skarn from the biotite-epidiorite. This shows the great tendency of lithium to enter the biotite lattice. Rb, Ba, Sr and Ag followed K. The amount of the K gained (4·14) is much higher than that of the Ca subtracted (1·56). It is understandable, therefore, why Sr, which can proxy for both K and Ca followed the former in this case. The total gain in combined Fe^2 and Fe^3 (0·76) is less than the loss in Mg (0·86). Correspondingly, the total gain in Li, V and Sc (0·05) is also less than the total loss in Ti, Mn, Cr, Co, Ni, Cu, Sn and Mo (0·26).

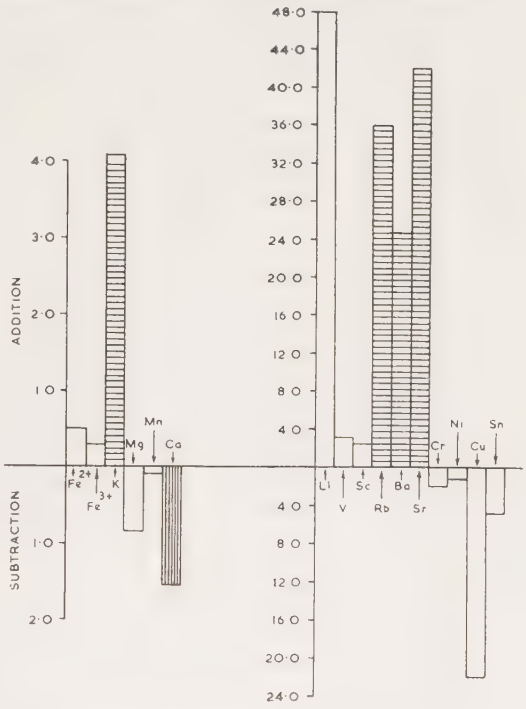

Fig. 2. Addition and subtraction (per rock "unit cell") of major and trace elements during the transformation of biotite-epidiorite (*B*) to biotite-skarn (*C*). The amounts in the case of the trace elements are multiplied by 1000.

Na was lost in accordance with the impoverishment in sodic plagioclase.

Ga and Al remained unchanged and therefore the ratio Ga/Al is the same. Table 5 shows that the transformation of biotite-epidiorite to biotite-skarn involved negligible change in the ratios Ni/Mg, Co/Mg and Co/Fe^2. These ratios are also approximately the same in the biotite-epidiorite and the epidiorite, suggesting that Ga, Ni and Co enter into the biotite and amphibole lattices with about equal ease. The Li/Mg ratio becomes much higher in the biotite-skarn. Notable changes take

place in the ratios of Ba, Rb and Sr to K. The ratio Rb/K increases markedly. Ba/K decreases slightly and (Rb + Ba)/K is higher in the biotite-skarn. Sr/K decreases but Sr/Ca increases. Rubidium is, therefore, the element which most readily replaces K in the biotite lattice.

(c) *Alteration of biotite-skarn C to lepidomelane-skarn D*

The biotite-skarn passes locally into lepidomelane-skarn. In other places, it is metasomatically transformed into chlorite-skarn.

The mica of the lepidomelane-skarn is different from that of the biotite-skarn. The lepidomelane has X = light golden yellow < Y = deep gold < Z = reddish gold; $2V = 20°$; $\gamma = 1{\cdot}681$; and marked dispersion; whereas the biotite of the biotite-skarn has X = straw yellow < $Y = Z$ = old gold to greenish brown; $2V$ small; and γ ranging from 1·643 to 1·645 ([7] p. 41 and p. 36). In association with the "golden" mica, the lepidomelane-skarn has a relatively small amount of biotite which is greenish brown, or distinctly green in colour, and displays optical properties resembling those of the biotite of the biotite-skarn. The textural relationship between the lepidomelane and the greenish biotite indicates that the former has developed at the expense of the latter. In places, the lepidomelane-skarn contains hastingsite relics of the original rock, that is, the epidiorite. Sphene occurs in minute granules as a minor accessory.

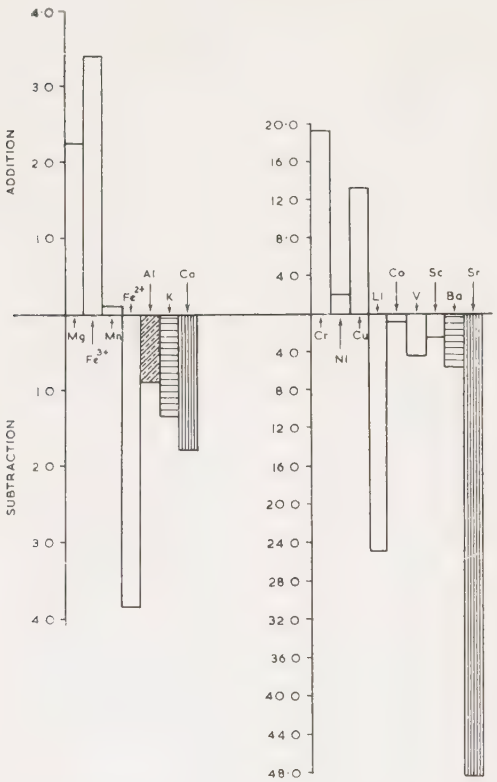

Fig. 3. Addition and subtraction (per rock "unit cell") of major and trace elements during the transformation of biotite-skarn (*C*) to lepidomelane-skarn (*D*). The amounts in the case of the trace elements are multiplied by 1000.

The dominant mineralogical change is evidently the transformation of biotite to lepidomelane.

The chemical changes in the major elements are shown in Table 3 and Fig. 3; the most significant changes involved addition of Fe^3 3·43, Mg 2·26 and Na 0·76 and subtraction of Fe^2 3·86, Ca 1·80, K 1·44 and Al 0·90.

The trace elements that increased are Ti, Mn, Cr, Cu and Sn; Ga; Rb and Pb; and Y. The trace elements that decreased are V, Sc, Co and Li; Ba and Ag; and Sr. Ti, Mn, Cr, Ni, Cu and Sn followed Mg and Fe^3, while Li, V and Sc followed Fe^2. Ba and Ag followed K and Sr followed Ca and possibly K. The total addition of Fe^3 and Mg (5·69) is higher than the total subtraction of Fe^2 (3·86). Concordantly, the total addition in Ti, Mn, Cr, Ni, Cu and Sn (0·3) is higher than the total subtraction of Li, Co, V and Sc (0·03). The total subtraction of Ba, Sr and Ag (0·05) exceeds that of the added Rb and Pb (0·009) in accordance with the decrease of K.

Na was added, although there was no development of soda-plagioclase. The sodium content of lepidomelane is generally higher than that of biotite. It can be present amongst the (X) group elements of the generalised mica formula (see below) or it may be replacing Fe^{3+} in the six-fold coordination positions.

Ga was added, yet Al was subtracted. This can be readily explained if we consider that the amount of the Al lost (0·90) is far less than the Fe^3 gained (3·43). Fe^3 can replace Al and Ga substitutes for both.

The transformation of biotite to lepidomelane does not involve a change in the lattice type. The general chemical formula for each of these micas is also of the same type. The formula of mica is known to be $(X)_{0-1}\,(Y)_{2-3}\,(Al, Si)_4\,O_{10}(OH, F)_2$, where (X) comprises K, Ca, Na, Rb, Ba and Sr; and (Y) is Al, Mg, Fe^2, Fe^3, Ti, Mn, Cr, Co, Ni and Li, all having coordination number six. The difference between lepidomelane and biotite is that the former has relatively more Fe^3 and less Mg and Fe^2. The total amounts of these elements would be essentially the same. It is significant that the total of the ratios* (Mn + Ni + Co + Li)/Mg, (Co + Li)/Fe^2 and Cr/Fe^3 in the biotite-skarn and the lepidomelane-skarn are 12·65 and 13·13 respectively. Moreover, the ratios (Sr + Rb + Ba)/K are 73·25 and 73·80 respectively. The similarity of these ratios in both rocks indicates that the trace elements enter with exactly the same ease into the identical lattices of both biotite and lepidomelane, replacing the appropriate major elements in the favourable positions of the structure. However, Sr/Ca differs widely in the two rocks. On the one hand, calcium is not nearly so important an element in biotite and lepidomelane as K, Mg, Fe^2, or Fe^3. On the other hand, the minor accessories in both rocks are mainly calcium-bearing minerals, such as epidote, sphene and apatite. Moreover CO_2 is 2·02 % in the biotite-skarn and none in the lepidomelane-skarn, normative calcite being 4·59 in the former. Strontium, therefore, is most likely to be present in the calcite and the other calcium-bearing minor accessory minerals.

(d) *Alteration of biotite-skarn C to chlorite-skarn E.*

Transitional rocks between the biotite-skarn and the chlorite are found in places. The chlorite-skarn is composed of chlorite (ripidolite), epidote, quartz, feldspar which may be iso-orthoclase (intimately intergrown with chlorite), a little albite, sphene and calcite ([7] p. 44).

The chemical changes (Table 3 and Fig. 4) in the major elements involve addition of Mg 1·22, Fe^3 0·26 and Na 0·26 and subtraction of K 4·36, Al 1·90 and Fe^2 0·50. The trace elements that increased are Ti, Mn, Li, Cr, Ni, Cu, Sn and Mo. The trace elements that decreased are Rb, Ba, Sr, Y and Ag; Ga; and V and Sc.

The general behaviour which has been found in all the previous transformations is also followed in this case. Ti, Mn, Li, Cr, Ni, Cu, Sn and Mo follow Mg and Fe^3. Rb, Ba, Sr and Ag follow K. Ga follows Al; and V and Sc follow Fe^2. The total addition of Mg and Fe^3 (1·48) exceeds that of the subtracted Fe^2 (0·50) just as the total addition of Ti, Mn, Li, Cr, Ni, Cu, Sn and Mo (0·49) exceeds the subtraction of V and Sc (0·008). The loss in K is far greater than the added Ca, thus explaining

* Li × 1000/Fe^2 and Mn × 10/Mg of the biotite-skarn and lepidomelane-skarn are 0·92 and 0·56, and 1·00 and 0·62 respectively. Ti/Mg was not taken since Ti is also present in sphene. The other ratios are recorded in table 5.

the behaviour of Sr. Na was added in accordance with the development of albite in the chlorite-skarn.

The chlorites in general are known to have more hydroxyl and less of the alkalies, mainly K, than the micas. The chlorite-skarn is richer in H and poor in K than both the biotite-skarn and the lepidomelane-skarn. In consequence of this, the Rb, Ba, Sr and Ag contents of the chlorite-skarn are much lower than those of the other two rocks and Pb is also very low. The main differences between the biotite-skarn on one hand, and the lepidomelane- and chlorite-skarns on the other, are (a) increase of Rb/K in the lepidomelane-skarn and its decrease in the chlorite-skarn and (b) the marked decrease of Sr/Ca, reaching its lowest value in the chlorite-skarn. Li/Mg decreases in the lepidomelane-bearing rock and is approximately the same in both the biotite- and the chlorite-bearing rocks. Cr/Fe^3 increases in the lepidomelane-skarn but is practically unaltered in the chlorite-skarn. Co/Fe^2 behaves somewhat like Cr/Fe^3, but decreases more notably in the chlorite-skarn.

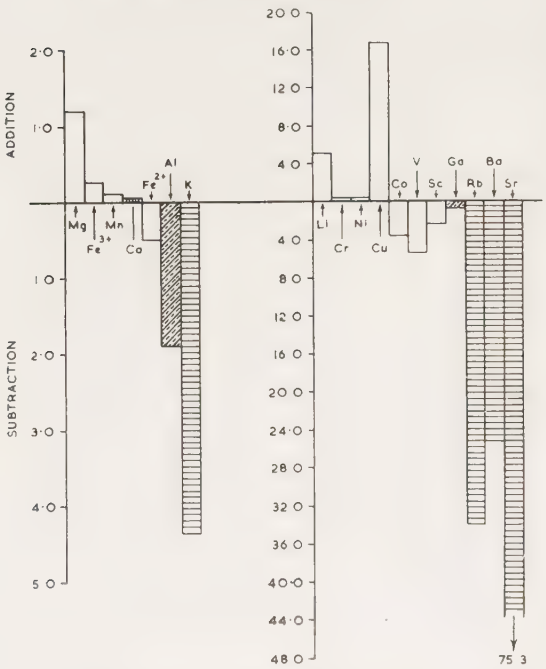

Fig. 4. Addition and subtraction (per rock "unit cell") of major and trace elements during the transformation of biotite-skarn (*C*) to chlorite-skarn (*E*). The amounts in case of the the trace elements are multiplied by 1000.

It is important to estimate the changes involved in the transformation of the biotite-skarn to its two metasomatic derivatives. Table 6 records the addition and subtraction of the different elements which have taken place where two "unit cells" of the biotite-skarn are assumed to have given rise to one "unit cell" of the lepidomelane-skarn and one unit all of the chlorite-skarn. There would then be a gain of Fe^3, Mg and Na, the added trace elements being Ti, Mn, Cr, Ni, Cu, Sn and Mo. There would also be a loss of Al; Fe^2; Ca; and K, the subtracted trace elements being Ga; Li, Co, V and Sc; Sr and Y; and Rb, Ba and Ag. The total gain in Fe^3 and Mg (3·59) exceeds the loss in Fe^2 (2·18),

Table 6. Gains and losses in biotite-skarn to give rise to both lepidomelane- and chlorite-skarns

Addition	*Subtraction*
1·89 Fe^3, 1·70 Mg, 0·51 Na, 9·58 H, 0·28 Ti, 0·06 P, 0·09 Mn, 0·01 Cr, 0·002 Ni, 0·01 Cu, 0·0003 Sn, 0·00002 Mo, 0·00005 Pb	0·03 Si, 1·40 Al, 2·18 Fe^2, 0·89 Ca, 2·90 K, 1·54 C, 0·0003 Ga, 0·005 Li, 0·002 Co, 0·005 V, 0·002 Sc, 0·06 Sr, 0·0002 Y, 0·01 Rb, 0·017 Ba, 0·0002 Ag, 0·003 Zr

corresponding to the total gains (0·39) and losses (0·02) of the trace elements which can proxy for these three interchangeable elements.

(e) *Alteration of epidiorite to skarn-rocks: General statement*

The cumulative sum of the different geochemical changes which have taken place in all the transformation processes discussed above is recorded in Table 7. On the whole, there has been increase in Mg and Fe^3 as well as their substituting minor and trace elements, namely, Mn, Cr, Ni, Li, Cu and Sn. K has been gained as were

Table 7. Cumulative gains and losses in epidiorite to give rise to the skarn rocks

Addition	*Subtraction*
1·90 Mg, 1·99 Fe^3, 2·23 K, 18·55 H, 1·08 C, 0·05 Li, 0·01 Cr, 0·002 Ni, 0·0003 Sn, 0·11 Mn, 0·30 P, 0·03 Rb, 0·017 Ba, 0·00005 Pb	2·13 Fe^2, 3·80 Al, 4·55 Na, 3·19 Ca, 2·49 Si, 0·001 Co, 0·003 V, 0·03 Ti, 0·00002 Mo, 0·0004 Ga, 0·03 Sr, 0·0002 Y

the trace elements which can proxy for it, namely, Rb, Ba and Pb. On the other hand, there has been decrease in Fe^2, and the minor and trace elements which replace it, namely, Ti, Co, Sc and Mo. Al and Ga have been subtracted. Sr and Y have followed Ca. The total gain in Mg and Fe^3 (3·89) is higher than the loss in Fe^2 (2·13) in correspondence with the totals of gains (0·17) and losses (0·04) in the trace elements which can proxy for these three elements. The loss in Ca exceeds the gain in K and thus the subtraction of Sr can be explained.

H has been gained in accordance with enrichment in the hydroxyl; and Na has been lost in accordance with the impoverishment of the soda plagioclase. The trace elements which follow Na cannot be recognised precisely. There has been a gain in C in agreement with the increase of calcite.

P has increased and Zr decreases. These two elements are found mainly in the minor accessory minerals apatite and zircon respectively. The role played by these minerals in the transformations is insignificant and therefore, P and Zr are not discussed.

The same behaviour is shown in some Finnish rocks studied by Sahama [12]. At Ihovaara Hill, "contaminated" rapakivi granite (IV) has been formed by metasomatic replacement of the mica-gneiss country-rock (I). The chemical and spectrographic analyses of his mica-gneiss (II) from the immediate vicinity of the rapakivi contact, and the contaminated rapakivi granite (IV) from the same contact are given by Sahama ([12] analyses II and IV Table XI, p. 59). The mica-gneiss (II) is relatively rich in Mg, Fe^2 and Fe^3. The corresponding trace elements which are also enriched in this rock are Ti, Mn, Cr, Ni, Co, Li and V. Ca; Sr and Y are also higher in the mica-gneiss. On the other hand, the contaminated rapakivi granite (IV) is enriched in K and the total of Rb and Ba also increases relative to the mica-gneiss (II).

Fig. 6 shows the changes in the proportions of (a) Rb, Ba and Sr, and (b) Cr + Li, Co and Ni in the different rocks of the White Cow sill near Malin Head. (a) Here the change has involved relative enrichment of both Rb and Ba, and relative impoverishment in Sr up to the biotite-skarn stage. Beyond this stage, two different

alterations have taken place. The one, giving rise to lepidomelane-skarn has involved an increase in Rb relative to Sr and only a slight change in Ba. The other, giving rise to chlorite-skarn has involved an increase in Ba relative to Rb and only a slight change in Sr. (b) There has been an increase in the relative proportions of the total Cr + Li and a relative decrease in Ni up to the biotite-skarn stage. Co also decreases but not so markedly as Ni. The increase in the total proportions of Cr + Li continues in the transformation of biotite-skarn to lepidomelane- and chlorite-skarns, with a relative decrease in Co in both rocks, but with a relative decrease in Ni in the lepidomelane-skarn and a relative increase in Ni in the chlorite-skarn.

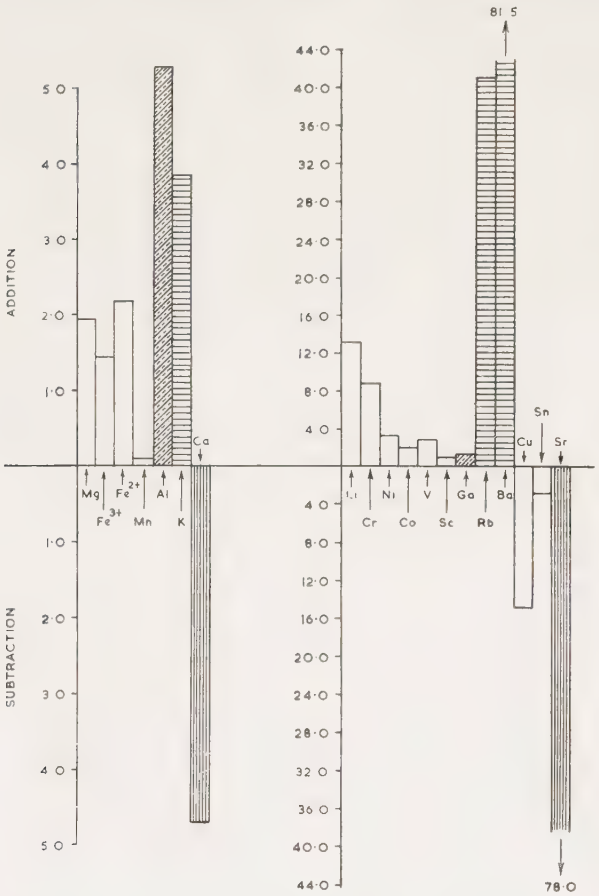

Fig. 5. Addition and subtraction (per rock "unit cell") of major and trace elements during the transformation of quartzite (*F*) to mica-schist (*G*). The amounts in the case of the trace elements are multiplied by 1000.

Alteration of Quartzite to Mica-Schist

The quartzite (No. 394) is composed of quartz and albite with a little potash feldspar, muscovite, biotite and garnet. It is relatively rich in calcite. In comparison with the quartzite the mica-schist is enriched in potash feldspar and biotite. It contains accessory apatite and iron-ore; calcite is absent or very scarce and garnet is found rarely.

The chemical changes expressed in terms of the "unit cells" of the rocks are given in Table 3 and Fig. 5. They involved addition of Al 5·32, Fe^2 2·18, Fe^3 1·44, Mg 1·95 and K 3·86 and subtraction of Ca 4·69 and Na 1·16.

The trace elements behave in essentially the same way as found in the transformation of the epidiorite to skarn rocks. Ti, Mn, Li, Cr, Co, Ni, V and Sc follow Mg, Fe^2 and Fe^3. Rb and Ba follow K. Sr follows Ca and Ga follows Al. Although Cu and Sn, which usually follow Mg and iron, were subtracted, the total of the subtracted amounts of these two elements (0·02) is far less than the total amounts of the added elements (0·65) which can proxy for Mg and iron. The same is true with respect to Pb and Ag, which substitute for K.

Changes in Tl, Mo, Ge and In are not detectable, since these elements if present are found in amounts below the limits of sensitivity.

Conclusions

Holmes and Reynolds [7] believe that the transformations discussed above may be correlated with the development of migmatitic rocks such as those outcropping to the west of the Malin Head district. The skarn rocks would be the basic front representatives of this granitization process. The total additions and subtractions

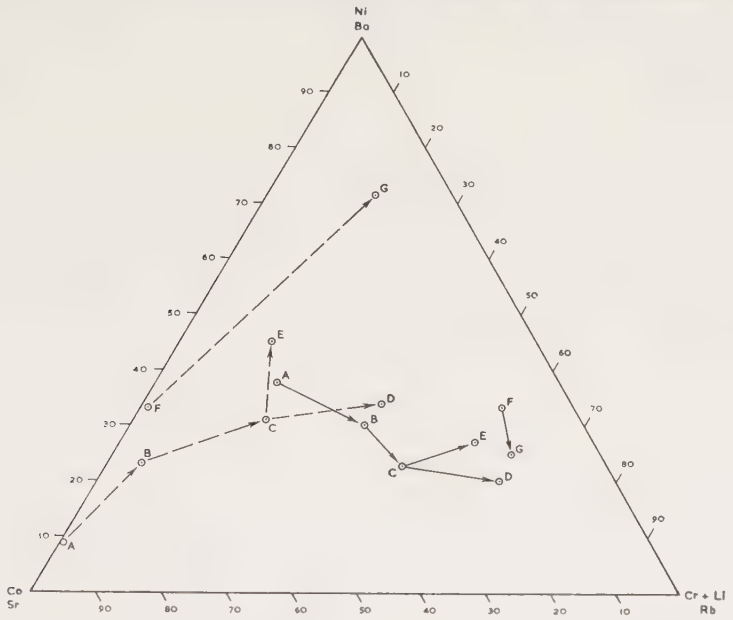

Fig. 6. Relative proportions of Ni, Co and Cr + Li (full line); and Ba, Sr and Rb (dotted line) in the analysed rocks. Notice that the trends in the transformation epidiorite to skarn-rocks with respect to change in the proportions of Ni, Co and Cr + Li; and Ba, Sr and Rb are respectively similar to those in the transformation quartzite to mica-schist. *A* epidiorite, *B* biotite-epidiorite, *C* iotbite-skarn, *D* lepidomelane-skarn, *E* chlorite-skarn, *F* quartzite and *G* mica-schist.

of the different elements during the transformation of epidiorite to skarn rocks as a whole, and that of quartzite to mica-schist are recorded in Table 8. The data show that K, Mg, Fe^2, Fe^3 and Al are added, and that they culminate in the basic front

Table 8. Cumulative gains and losses in epidiorite plus quartzite to give rise to skarn rocks plus mica-schist

Addition	*Subtraction*
1·52 Al, 3·43 Fe^3, 0·15 Fe^2, 3·85 Mg, 6·09 K, 27·43 H, 0·0006 Ga, 0·48 Ti, 0·44 P, 0·22 Mn, 0·06 Li, 0·02 Cr, 0·001 Co, 0·005 Ni, 0·0005 V, 0·06 Rb, 0·09 Ba, 0·002 Y	5·99 Si, 7·88 Ca, 5·71 Na, 3·53 C, 0·1 Sr, 0·0003 Ag, 0·001 Pb, 0·005 Cu, 0·002 Sn

rocks. The minor elements, Ti, P and Mn also culminate in the basified rocks as discovered by Reynolds [11]. The present study shows that the trace elements which proxy for K, Mg, Fe^2, Fe^3 and Al culminate in the same rocks as those which show culmination of the major elements. Rb and Ba culminate with K; Li, Cr and Ni with Mg and Fe^3; Co and V with Fe^2; and Ga with Al.

The released elements after the formation of these basified rocks are Si, Ca and one of the alkalies which is Na in this case. Sr was released in accord with Ca. There has also been release of Sn, Ag, Pb and Cu. These are elements commonly found in the ore-deposits associated with granitic rocks. If the hypothesis of the metasomatic derivation of granitic rocks is true, it might be suspected that ore-deposits composed of Sn, Ag, Pb and Cu could be obtained from the country-rock material. Further geochemical work is needed in order to establish the quantitative validity of this assumption.

Acknowledgement—I wish to express my grateful thanks to Dr. D. N. McArthur, Director of the Macaulay Institute for Soil Research at Aberdeen, for his kindness in allowing the spectrographic determination to be made there; to Drs. R. L. Mitchell and R. O. Scott of the Macaulay Institute for their valuable help and guidance during the spectrographic analysis; to Prof. A. Holmes and Dr. D. L. Reynolds for providing the analysed materials and for their constructive critisism and discussion; to Dr. Th. G. Sahama for reading and critisising the manuscript; and to Prof. L. R. Wager for his valuable suggestions.

References

[1] Ahrens, L. H.; The unique association of thallium and rubidium in minerals. J. Geol. 1948 **56** 578–590. [2] Barth, Tom F. W.; Oxygen in rocks: A basis for petrographic calculations: J. Geol. 1948 **56** 50–60. [3] Buerger, M. J. and Washkin, E.; Metamorphism of minerals. Amer. Mineral. 1947 **32** 296–308. [4] Goldschmidt, V. M.; Drei Vortrage über Geochemie. Geol. Fören. Stockholm Förhandl. 1934 **56** 385. [5] Goldschmidt, V. M.; The principles of distribution of chemical elements in minerals and rocks. J. Chem. Soc. for 1937 655. [6] Goldschmidt, V. M.; The geochemical background of minor element distribution: Soil Sci. 1945 **60** (No. 1) 1–7. [7] Holmes, A. and Reynolds, D. L.; A front of metasomatic-metamorphism in the Dalradian of Co. Donegal. Comm. Géol. Finlande Bull. 1947 **140** 25–65. [8] Jaffe, H. W.; The role of yttrium and other minor elements in the garnet group: Amer. Mineral. 1951 **36** 133–155. [9] Mitchell, R. L.; The spectrographic analysis of soils, plants and related materials. Commonwealth Bur. of Soil Sci., tech. comm. No. 44 (1948) pp. 53–77. [10] Nockolds, S. R. and Mitchell, R. L.; The geochemistry of some Caledonian plutonic rocks: A study in the relationship between the major and trace elements of igneous rocks and their minerals. Trans. Roy. Soc. Edin. 1948 **61** (Part II) 533–575. [11] Reynolds, D. L.; The sequence of geochemical changes leading to granitization. Quart. J. Geol. Soc. 1946 **102** 389–446. [12] Sahama, Th. G.; On the chemistry of the east Fennoscandian rapakivi granites: Comm. Géol. Finlande Bull. 1945 **136** 15–67. [13] Wickman, F. E.; Some aspects of the geochemistry of igneous rocks and of differentiation by crystallization. Geol. Fören. Stockholm Förhandl. 1943 **65** 371–396.

Geochimica et Cosmochimica Acta, 1952, Vol. 2, pp. 185 to 206. Pergamon Press Ltd., London

The geochemistry of indium

D. M. Shaw

Department of Geology, McMaster University, Hamilton, Ontario, Canada

(Received 31 October 1951)

ABSTRACT

A double-arc spectrochemical procedure was used to analyse numerous minerals and rocks for indium. The method had sensitivity of the order of 0·02 ppm In with precision of ±20%.

Among the minerals, indium occurs in low concentrations in most mafic silicates due to the $In^{+3}-Fe^{+2}$ diadochism. It is absent from felsic silicates. Others have reported In enrichment in sphalerite and other sulphides, and a common association of In and Sn.

In igneous rocks In is distributed very erratically, suggesting the possibility of the existence of indium provinces, or alternatively that In is present in accessory sulphides.

Argillaceous sediments contain a little In, deposited by oxidation and hydrolysis of eroded material. Strong reducing environments cause the slight In-enrichment in carbonaceous rocks.

The crustal abundance of In is 0·11 ppm. The probable distribution of In throughout the earth is briefly discussed from thermochemical data.

Introduction

Indium was discovered by F. Reich and T. Richter in 1863, during the examination of a Freiberg sphalerite. Traces of thallium were being sought for but the spectroscope failed to show the green thallium line, revealing instead an indigo-blue line which had never before been observed. A new element was extracted and named "indium" from this prominent spectral line.

Indium is a heavy metal of low melting-point (155° C) which is never found uncombined in nature. It has been placed in the third group of the periodic table, between gallium and thallium, by reason of its atomic weight and its resemblance to these elements and aluminium. Thus, indium alums have been prepared, isomorphous with corresponding alums of aluminium, gallium and thallium; also, indium hydroxide shows amphoteric properties similar to aluminium hydroxide.

The first indium extracted came from a sphalerite and since that time numerous authors have reported the presence of indium in this mineral (see Mellor [26], p. 387). Erämetsä [13] has shown that indium has a strong tendency to concentrate in zinc blende rather than in any other mineral. Zinc blende is the source of indium at the present time and there is a growing industrial demand for the metal (see Ludwick [24]). It is, nevertheless, very rare and seldom occurs in concentrations greater than 0·1%. Indium is, however, found in other sulphides, having a strongly chalcophile character. Hartley and Ramage [18] showed that indium is frequently present in other minerals, notably iron, manganese, tin and aluminium ores, and is actually a widely distributed element. Hörmann and Goldschmidt [17] found indium in common silicate rocks, though in very small amounts.

Few of the analytical methods to determine indium are suitable for geological materials, unless elaborate extraction and concentration procedures are followed. The spectrograph is the most convenient tool but seldom has sufficient sensitivity

to detect indium in any but the richest samples. Workers at Hamburg, however, evolved techniques whereby the indium (and other volatile elements) could be fractionally distilled from a rock or mineral sample and then analysed spectrographically. Thus, Ottemann [30] heated the sample in an auxiliary furnace and condensed a sublimate containing the volatile metals. This was then transferred to the boring in a graphite electrode and analysed by a D.C. arc method. Preuss [31] used a similar technique but distilled the volatiles directly into a D.C. arc through a hollow cathode. The principle of these methods was embodied in the technique used in the present investigation.

In a recent study on the abundance and distribution of thallium (Shaw [38]), analyses were also carried out for indium. Although there is a fairly substantial literature on the distribution of indium few quantitative determinations have been made, so that previous figures for the abundance of indium were guesses, rather than calculations. The results of the present work permit rather more precise discussion of the quantitative distribution of indium, although the results can only be regarded as provisional, as will be seen later.

The materials used for analysis in this study came from many sources, and the writer is indebted to numerous geologists and institutions for their kindness. In particular the Finnish samples were kindly given to me by Dr. Kalervo Rankama, and came from the same hand-specimens as samples used in his investigations of niobium and tantalum geochemistry [33], [34]. The assistance and encouragement of Dr. Rankama and Mr. Oiva Joensuu at the University of Chicago are deeply appreciated. I am further indebted to the University of Chicago for the award of a Salisbury Fellowship, which enabled this work to be carried out. Dr. Rankama and Dr. H. S. Armstrong have given numerous suggestions concerning the manuscript.

Methods

The procedures used to determine indium in the materials under study were identical with those used for thallium, and an abbreviated description will suffice. For further details reference may be made to previous papers (Shaw, Joensuu and Ahrens [39]; Shaw [38]). Briefly, a spectrochemical method was used with a double-arc procedure, to obtain the high sensitivity necessary for determination of the very minute quantities of indium in common rocks and minerals.

When analysing a rock by a D.C. arc method, a fractional distillation procedure will increase the sensitivity for a readily volatile element such as indium. Lowering the arc temperature by mixing the sample with a flux, usually of an alkali, salt, achieves this most effectively. Another factor which can aid the fractional distillation of the analysis element is the presence of a "carrier agent." In this work ammonium chloride was found suitable as carrier agent and was mixed with lithium carbonate, the latter serving as flux. Another factor which has bearing on the sensitivity is the absolute amount of the element present in a given sample. The greater the absolute amount the easier it is to determine (in "trace" quantities, that is). It is therefore important to use as large a sample as is practical. The double-arc principle is of value here, as samples up to half a gram and more can conveniently be analysed. Further details of the method are given in Table 1, and in the papers cited above.

In general it is not possible to obtain precise analyses by spectrographic methods, unless the sample in each case is of similar bulk composition and physical state. The excitation of the analysis elements is strongly influenced by the presence of other elements in varying quantities. The procedures were therefore set up to provide as precise figures as possible for silicate rocks, which are quantitatively the most important. It must therefore be borne in mind throughout the following discussion that the figures for other materials cannot be assumed to have the same precision as for the silicates. Nevertheless, two factors tend to minimise the errors for these other materials. First, the alkali-rich flux stabilizes the excitation conditions, thereby compensating to some extent for variations in bulk composition. Secondly, an internal standard (tin) was used, with similar volatility and ionisation potential to indium, thus compensating both for random variations in excitation, and for systematic variations due to varying sample composition.

Samples were crushed and sieved to pass 150 mesh silk bolting-cloth, taking the usual precautions in sampling. Possible contamination was avoided at all stages in the preparation of flux and samples, as the quantities to be determined were so minute. Flux and analysis materials were mixed by homogenising in an agate mortar.

For the evaluation of analyses it was necessary to prepare a set of standards, containing indium in known concentrations. For the base material of these standards a mixture of silica glass, olivine and bytownite in equal proportions was prepared. Each of these materials, and the flux, was subjected to a blank arcing, in order to confirm that in all cases indium and tin were below the limits of detection. They were ground to pass a 200 mesh sieve and then mixed carefully. Using this base material and the *Johnson-Matthey* Specpure Indium oxide a series of standards was prepared, containing indium in concentrations from 1000 ppm to 0·32 ppm, in steps of 1:0·316.

Two indium lines were necessary to cover the whole range of standard concentrations, but in the analyses all concentrations fell within the range of the more sensitive line. Each was checked for absence of interfering coincidences.

The densities of recorded lines were measured, and a calibration curve was constructed for each plate, using a six-step sector and measuring a line free from background and self-reversal. A six-step spectrum of each analysis exposure was also obtained, and the densities of the analysis and internal standard lines and their backgrounds measured at suitable levels. A calculating-board was employed to facilitate arithmetic, and the methods of Honerjäger-Sohm and Kaiser [20] were followed. In this procedure the galvanometer reading A and A_0 for the spectral line and for an unexposed part of the plate respectively, are converted to the quantity W, where

$$W = \log\left(\frac{A_0}{A} - 1\right).$$

For plate calibration the W-values are plotted against Y, where $Y = \log I$ and $I =$ intensity of emitted light. Then the ratio of intensities of the analysis line I_z and internal standard line I_s is measured on the abscissa as $dY_{z,s}$ (after background correction) where,

$$dY_{z,s} = \log\frac{I_z}{I_s} = \log I_z - \log I_s = Y_z - Y_s.$$

To obtain the working curve the standards were arced, values of dY calculated and these figures plotted against the logarithm of concentration (see Fig. 1). The upper working limit on the "A" curve was about 10 ppm.

Due to excitation instability in the double-arc method as used at present (see Shaw, Joensuu and Ahrens ([39], p. 235) a rather high reproducibility error was expected, and is shown by the distribution of points in the standard curves (Fig. 1). The R.M.S. deviation is $\pm 30\%$ so analyses were run in duplicate, thereby decreasing the error to $\pm 20\%$. However it is probable that the precision of most analyses was somewhat better than this figure, since the size of the R.M.S. deviation was due mostly to occasional wide fluctuations, and the majority of the deviations were less.

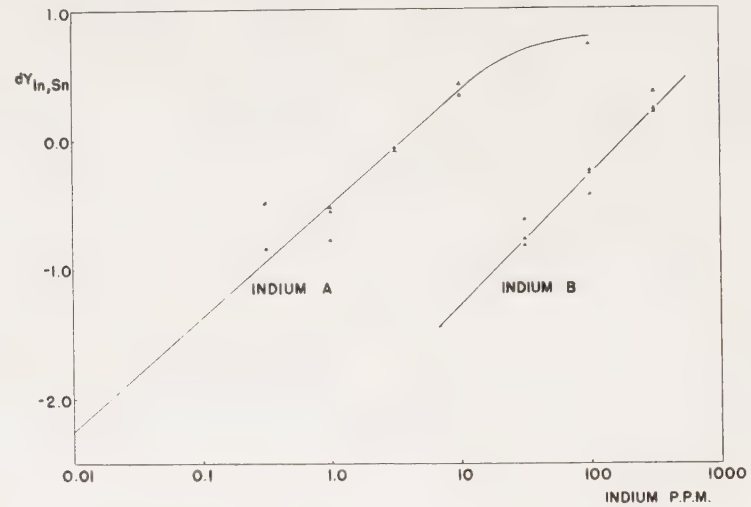

Fig. 1.

The sensitivity limit is a rather arbitrary quantity, depending mainly on the density of the internal standard line, but partly on the background level, thus differing for each exposure. Hasler and Kemp [19] take the limit of measurement as the concentration for which the analysis line has an intensity of 0·3 times the background intensity. This is an arbitrary value, since the line can sometimes be observed at lower intensities, but is close to the limiting value for precise photometry. Using this relation the sensitivity limit was usually between 0·01 and 0·07 ppm, and extrapolation of the standard curve to this range was permissible.

An average figure for the sensitivity limit was 0·02 ppm with a precision error of $\pm 20\%$.

The results of the analyses appear in Table 2, expressed in parts per million to two significant figures. Since the concentration scale was logarithmic the second figure is always retained, even when it expresses thousandths of one ppm. This procedure is logical, but the value of the second figure is no doubt of little significance at low concentrations. It will be noticed that certain analyses appear twice in the table, since certain materials, *e.g.* anorthosite, may be considered as having both mineralogical and petrological significance. The symbol "—" indicates an indium content below the limits of detection.

Table 1. Arcing procedure for indium with the double-arc method

Spectrograph	21-foot grating instrument by *Jarrell-Ash Company* with Wadsworth type mounting: dispersion 5 Å/mm in first order spectrum
Power Source	Emitator by *Bolidens-Gruv AB*, Sweden
Voltage	225 v D.C.
Current	7 amp
Electrodes	Anode (Upper), 1/8″ diameter graphite rod (*National Carbon Company*, "Special" Grade) Cathode (Lower), 3/16″ diameter graphite rod (*National Carbon Company*, "Special" Grade) Furnace (*National Carbon Company*, "Regular" Grade). Dimensions in Shaw, Joensuu and Ahrens [39]
Arc Gaps	Upper 9 mm Lower 2 mm
Slit	Length 12 mm: width 30 microns
Step-Sector	Seven-Step sector by *Jarrell-Ash Company:* step-ratio 1:2
Optical System	Arc focussed on a diaphragm by a short-focus spherical lens. Its image was focussed on the spectrograph mirror by a long-focus cylindrical lens placed just in front of the slit
Exposure	90 sec
Plates	*Eastman-Kodak* No. 103–F and 103–0
Developing	No. 103 F—3 min at 20° C in Developer D–19 No. 103 0—4 min at 20° C in Developer D–19
Sample	One part of flux (1 NH_4Cl+3 Li_2CO_3+ internal standard) homogenised in an agate mortar with three parts of the rock sample, previously dried at 105° C. Total weight of the sample usually 560 mg, containing 0·5% SnO_2
Spectrum Lines	In 4511·323 Å—Indium "A" In 2932·624 Å—Indium "B" Sn 4524·741 Å Sn 3032·775 Å
Photometer	*Leeds and Northrup* Recording Photodensitometer

Indium in Minerals

A study of the first section of Table 2 indicates the rarity of indium in all the commoner minerals. Although the varieties analysed comprise only a small number of the different mineral kinds, other investigators have found that no mineral contains more than 1 % In, with certain doubtful exceptions, and it can therefore be described as a "dispersed" element (Vernadsky [42]). In the present study the highest concentration of indium was 5·8 ppm in hornblende from an unknown source. It follows that the crust of the earth contains little indium. On a later page it will be shown that the crustal abundance of indium is 0·11 ppm, and in the following pages any statement concerning enrichment or impoverishment in indium will imply this figure as reference.

The group of minerals analysed can be regarded as complementary to the results of Erämetsä [13], a work to which continual reference will be made in the course

Table 2. Analyses of rocks and minerals for indium

Sample Number	*Sample*	*Locality*	In *ppm*
		MINERALS	
		Native elements	
S 69	Graphite	Kärpälä, Mäntyharju, Finland	0·028
S 152	Graphite	Blackdonald Mine, Renfrew Co., Ontario . .	—
		Oxides and Hydrated oxides	
S 99	Quartz	Custer Mt., Black Hills, S. Dakota	—
S 129	Opal	Grand Manan Is., New Brunswick, Canada .	—
S 116	Magnetite	Seabrook Lake Mississagi Reserve, Ont. (extracted from Lamprophyre S 12) . . .	0·071
S 20	Hematite	Pöpönsaari, Suojärvi, K.F.S.S.R.	—
S 19	Limonite	Haapakylä, Evijärvi, Finland	—
S 154	Iron Oxides	Säppi, Luvia, Finland (extracted from Diabase S 138)	0·12
S 170	Pyrolusite	(not known)	—
		Sulphides	
S 173	Pyrite	Crystal Falls, Michigan (see Slate S 174) .	—
S 131	Pyrrhotite	Creighton Mine, Sudbury, Ontario	—
S 134	Chalcopyrite	Creighton Mine, Sudbury, Ontario	4·8
S 135	Sphalerite	Beck Mine, Pitkäranta, K.F.S.S.R.	—
S 132	Marcasite	Veules, Normandy	—
S 136	Galena	Sakkijärvi, Finland	0·91
S 133	Molybdenite	Temagami, Ontario	—
		Halides	
S 127	Fluorite	Cardiff Tp., Ontario	—
S 4	Halite	Grand Saline Salt Dome, Texas	—
S 3	Sylvinite	near Carlsbad, New Mexico	—
		Phosphate	
S 101	Apatite	Custer Mt., Black Hills, S. Dakota	—
		Silicates	
		a) Nesosilicates	
S 139	Olivine rock	S. Massif, Khabozero, Kola Peninsula, U.S.S.R.	—
S 180	Olivine rock	(not known)	—
S 165	Almandine	Koirinkoski, Kitilä, K.F.S.S.R.	0·026
S 42	Garnet	Adirondacks, N. Y.	0·10
S 46b	Garnet	N. Stromfjord, Greenland.	0·18
S 167	Epidote	(not known)	0·59
S 168	Staurolite	(not known)	0·011
S 128	Zircon	Mt. Titanium, Georgia, U.S.A.	—
S 123	Titanite	Eganville, Renfrew Co., Ontario	—
		b) Inosilicates	
S 47	Hypersthene	Rifkol, W. Greenland	0·038
S 11	Hypersthene	Stillwater Complex, Montana	0·017
S 124	Diopside	Ojamo, Lohja, Finland	—
S 115	Augite	Seabrook Lake, Mississagi Reserve, Ont. (separated from Lamprophyre S. 12) . . .	0·31
S 122	Tremolite	Lee, Massachusetts	—
S 169	Hornblende	(not known)	5·8

Table 2. (Continued)

Sample Number	*Sample*	*Locality*	In *ppm*
		c) Phyllosilicates	
S 94	Muscovite	Kuutelokallio, Kaatiala, Kuortane, Finland	4·5
S 102	Muscovite	Custer Mt., Black Hills, S. Dakota	-
S 95	Phlogopite	Skräbböle, Parainen, Finland	
S 175	Biotite	(not known)	-
S 96	Lepidolite	Custer Mt., Black Hills, S. Dakota	—
S 172	Chlorite	(not known)	-
S 18	Kaolin	Werran Hills, Nigeria	0·12
S 14	Kaolin	Skräbböle, Parainen, Finland	-
		d) Tektosilicates	
S 99	Quartz	Custer Mt., Black Hills, S. Dakota	-
S 166	Nepheline	(not known)	
S 130	Leucite	Civita Castellano, Italy	
S 25	Calcic Plagioclase	Hange, Egersund, Norway	—
S 9	Calcic Plagioclase	Stillwater Complex, Montana	—
S 10	Calcic Plagioclase	Stillwater Complex, Montana	—
S 181	Bytownite	(not known)	-
S 40	Albite	High Climb, Black Hills, S. Dakota	-
S 98	Cleavelandite	Custer Mt., Black Hills, S. Dakota	—
S 126	Amazonite	Woodcox Mine, N. Hastings Co., Ontario	—
S 100	Microcline-Perthite	Custer Mt., Black Hills, S. Dakota	—
S 41	Microcline-Perthite	High Climb, Black Hills, S. Dakota	—
		e) Miscellaneous	
S 125	Beryl	Lyndoch Tp., Renfrew Co., Ontario	—
S 97	Tourmaline	Custer Mt., Black Hills, S. Dakota	—
		Igneous Rocks	
S 139	Olivine rock	S. Massif, Khabozero, Kola Peninsula, U.S.S.R.	—
S 25	Anorthosite	Hange, Egersund, Norway	-
S 9	Anorthosite	Stillwater Complex, Montana	
S 143	Pyroxenite	Webster, N. Carolina	—
S 63	Hornblendite	Kaalamo, Finland	0·053
S 21	Peridotite	St. George, Garden Cove, Aleutian Is.	—
S 24	Olivine-Basalt	St. Paul, Aleutian Is.	0·124
S 23	Basalt	Tolstoi Point, St. George, Aleutian Is.	0·32
S 71	Basalt	St. George, Aleutian Is.	0·26
S 90	Basalt (carrying native iron)	Disco Is., Greenland	0·13
S 112	Leucite-Basalt	Laacher See, Rheinprussen	0·19
S 113	Tephrite	Rheinprussen	
S 61	Gabbro	Peuhkurinmäki, Parikkäla, Finland	
S 137	Gabbro	Sudbury, Ontario	
S 140	Gabbro	Virnikkasokka, Moskuvaara, Sodankylä, Finland	
S 141	Gabbro	Duluth, Minnesota	0·013
S 142	Hornblende-Gabbro	Salem, Massachusetts	
S 138	Olivine-Diabase	Säppi, Luvia, Finland	0·078
S 57	Diabase-Pegmatite	Säppi, Luvia, Finland	0·30
S 144	Andesite	Mt. Shasta, California	

Table 2. (Continued)

Sample Number	*Sample*	*Locality*	In *ppm*
S 145	Diorite	Jersey City, New Jersey	—
S 147	Monzonite	San Juan Co., Colorado	
S 120	Tonalite	Marquis Tp., Ontario	
S 121	Tonalite	Dack Tp., Ontario	
S 22	Dacite	St. George, Aleutian Is	—
S 56	Oligoclase-Granite	Orijärvi, Kisko, Finland	
S 52	Granite-Gneiss	Petäjäkylä, Pitkärantä, K.F.S.S.R.	—
S 114	Granite	Hangö, Finland	—
S 53	Granite	Juva, Espoo, Finland (Bodom granite)	0·42
S 51	Granite	Maarianvaara, Finland	—
S 49	Granite	Sodankylä, Finland (Nattanen granite)	
S 54	Granite	Åva Brändo, Finland (Ava granite)	—
S 55	Granite	Bomarsund, Ahvenanmaa, Finland (Rapakivi)	2·0
S 48	Granite	Uuksu Salmi, K.F.S.S.R. (Rapakivi)	—
S 50	Granite	Bamböle, Vehkalahti, Finland (Rapakivi)	0·14
S 92	Pegmatite	Pyterlahti, Säkkijärvi, Finland (Rapakivi)	—
S 150	Obsidian	Millard Co., Utah	—
S 149	Obsidian	Lake Co,. Oregon	—
S 29	Granite Dyke	Albany Co., Wyoming	—
S 12	Lamprophyre	Seabrook Lake, Mississagi Reserve, Ont.	0·071
S 59	Lamprophyre	Åva Brändö, Finland	0·017
S 118	Syenite	Marquis Tp., Ontario	—
S 119	Syenite	Marquis/Otto Tps., Ontario	—
S 146	Phonolite	Cripple Creek, Colorado	—
S 164	Nepheline-Syenite	Methuen Tp., Ontario	—
S 58	Ijolite	Iivaara, Kuusamo, Finland	
		Sedimentary Rocks	
S 65	Limestone	Limberg, Parainen, Finland	—
S 64	Dolomite	Valkeamäki, Tiutia, K.F.S.S.R.	—
S 148	Arkose	Fair Haven, New Haven, Connecticut	—
S 93	Sandstone	Huvitus, Yläne, Finland	—
S 91	Phosphorite-Glauconite-Sandstone	Tallinn, Estonia	—
S 171	Bauxite	Tennessee	0·17
S 17	Laterite	Funchal, Madeira	0·058
S 38	Greywacke	Manitou Lake, Ontario	0·049
S 37	Greywacke	Mena, Arkansas	0·033
S 36	Greywacke	Washington State, U.S.A.	0·23
S 2	Loess	Farmdale, Illinois	0·051
S 1	Varved Clay	Pembina Co., N. Dakota	0·053
S 15	Clay	Mga River, Ingrai, U.S.S.R. (Yoldia clay)	0·012
S 16	Clay	Oulu, Finland (Ancylus clay)	0·054
S 8	Shale	East Hoosick, New York	
S 39	Argillite	Dickinson Co., Michigan	
S 13	Shale (lime-rich)	Grayville, Illinois	—
S 7	Slate	Eagle Bridge, New York	0·037
S 174	Pyritic Slate	Crystal Falls, Michigan	0·037
S 117	Shale	Tallinn, Estonia (Dictyonema shale)	0·18
S 66	Phyllite	Tähtinen, Aitolahti, Finland (Corycium phyllite)	tr. 0·06
S 67	Carbonaceous Schist	Beresford Lake, Manitoba	

Table 2. (Continued)

Sample Number	*Sample*	*Locality*	In *ppm*
S 68	Shungite	Veljakkala, Soanlahti, Finland	0·007
S 153	Anthracite	Schuylkill Co., Pennsylvania	—
S 151	Anthraxolite	Sudbury, Ontario	0·21
S 35	Porcellanite	Iron Co., Michigan	0·27
S 4	Rock Salt	Grand Saline Salt Dome, Texas	—
S 3	Sylvinite	near Carlsbad, New Mexico	—
S 5	Insoluble residue from Rock Salt	See S 4	—
S 6	Cap Rock	Hockley Mine Salt Dome, Texas	—
		Deep-Sea Sediments	
S 103	Manganese Nodule	11° N; 113° 48′ W; depth 4090 m	tr.
S 104	Volcanic Glass	11° N; 113° 48′ W; depth 4090 m	0·063
S 105	Iron-Manganese-rich Ooze	07° 40 N; 106° 21′ W; depth 3725 m	—
S 106	Globigerina Ooze	02° 44′ S; 92° 45′ W; depth 3600 m	—
S 107	Deep-Sea Clay	15° 40′ N; 123° 21′ W; depth 4300 m	0·085
S 108	Red Clay	08° 25′ N; 128° 48′ W; depth 4610 m	0·074
S 109	Siliceous Ooze	03° 05′ N; 133° 06′ W; depth 4370 m	--
S 77	Clay	36° 16′ N; 70° 09′ W; depth 4500 m	—
S 78	Clay	37° 42 N; 70° 53′ W; depth 3900 m	0·28
S 79	Clay	39° 25′ N; 69° 40′ W; depth 2480 m	—
S 80	Clay	39° 47′ N; 69° 42′ W; depth 1555 m	—
		Metamorphic Rocks	
S 62	Amphibolite	Impilahti, K.F.S.S.R.	—
S 26	Norite Gneiss	Albany Co., Wyoming	0·16
S 27	Diorite Gneiss	Albany Co., Wyoming	0·090
S 28	Quartz Diorite Gneiss	Albany Co., Wyoming	—
S 30	Quartz-Monzonite Gneiss	Albany Co., Wyoming	1·9
S 31	Granodiorite Gneiss	Albany Co., Wyoming	0·88
S 110	Granodiorite Gneiss	Egedesminde, Greenland	—
S 111	Hornblende Gneiss	S. Stromfjord, Greenland	—
S 70	Enderbite Gneiss	N. Isortog, Greenland	—
S 33	Garnet Gneiss	N. Isortog, Greenland	1·8
S 32	Garnet Gneiss	N. Isortog, Greenland	0·38
S 34	Granulite Gneiss	N. Isortog, Greenland	0·070
S 155	Olive Slate	Clove Quadr., New York	—
S 157	Black Phyllite	Moores Mills, New York	—
S 156	Black Phyllitic Slate	Clove Quadr., New York	0·050
S 158	Biotite Phyllite	Clove Quadr., New York	—
S 159	Biotite-Muscovite Phyllite	Clove Quadr., New York	0·066
S 160	Garnetiferous Schist	Clove Quadr., New York	0·46
S 162	Biotite-Garnet Schist	Clove Quadr., New York	
S 161	Biotite-Hornblende Schist	Danbury Quadr., New York	0·090
S 163	Garnet Schist	Clove Quadr., New York	0·32
S 176	Sillimanite Schist	Clove Quadr., New York (Dark Layer)	0·15
S 177	Sillimanite Schist	Clove Quadr., New York (Light Layer from S 176)	0·065

Table 2. (Continued)

Sample Number	*Sample*	*Locality*	In *ppm*
		Miscellaneous	
S 74	Meteorite	Holbrook, Navajo Co., Arizona (Chondrite) .	—
S 75	Meteorite	Norton Co., Kansas (Achondrite)	—
S 76	Meteorite	Plain View, Hale Co., Texas (Chondrite) . .	—
S 73	Caliche	Chile	—
S 81	Ocean Salts	Woods Hole Harbour, Massachusetts; surface	—
S 82	Ocean Salts	34° 36′ N; 30° 00′ E; depth 750–1325 m . .	—
S 83	Ocean Salts	34° 36′ N; 30° 00′ E; depth 1500–1900 m . .	—
S 84	Ocean Salts	40° 15′ N; 25° 19° E; depth 100–350 m. . .	—
S 85	Ocean Salts	40° 15′ N; 25° 19′ E; depth 350–750 m . .	—

of this paper. Bearing in mind that the limit of sensitivity of Erämetsäs method was 1 ppm In, and that his evaluation was semi-quantitative, the similarity to his mineral analyses is striking. Very few minerals contain more than 1 ppm, and the lower sensitivity limit of the present work allows some further details to be added to Erämetsäs discussion.

When a trace-element such as indium is detected in a mineral it is usually present in one of two situations. Either it is contained in inclusions of another mineral, or it must occupy a lattice site in the principal mineral. However it is also possible that the element is held by adsorption or other surface effects or is concealed within the mineral in some "cavity" or structural defect. These last are unlikely for most elements however, and can usually be neglected. It is not likely that many inclusions of another mineral are present, as steps were taken to obtain as satisfactory separations as possible. However ultra-microscopic inclusions are present in the purest mineral, and it is always possible that an element present only in very small traces may be carried by these unknown inclusions.

Trace elements in the minerals are commonly held in a structural position usually occupied by a major element of similar size, valency and chemical properties. The laws governing this camouflage were first enunciated by Goldschmidt (*e.g.* [16]) and amplified by Wickman [43], and as the principles will be familiar to the reader it is not necessary to give a recapitulation here.

In Table 3 are given the ionic radii for trivalent indium and the other metals (in their usual valency states in rocks) lying within ±15% of that value. Minerals which contain any of these other metals should then be able to carry indium in their place, with two provisos. Firstly, the metal being replaced must be chemically similar, especially so far as bonding is concerned. Secondly, another substitution may be necessary to balance the valencies, *e.g.* if In^{+3} replaced Zn^{+2} in sphalerite a second substitution of a different kind is necessary, or the unit cell has excess positive charge. Table 2 shows that among the silicate minerals the only ones which contain detectable indium are the mafics, with a single exception (kaolin). Moreover zircon, apatite, lepidolite, titanite, and the feldspars do not contain any detectable indium, so we may doubt whether the elements Li, Hf, Zr, Na, Lu, Ce, Yb, Ca and Y are vicarious with indium. This is to be expected, since these elements are chemically very different to indium. In the silicates then, it is evident that the present analyses

do not conflict with GOLDSCHMIDTs [17] conclusions, namely, that indium follows divalent iron and possibly divalent manganese. ERÄMETSÄ has also recorded the former replacement, but found that very few manganese minerals contained any determinable values. He also observed that the replacement of iron by indium does not apparently extend to the iron sulphides, as is found here also. The absence of indium in zircon and scandium-rich minerals was observed by ERÄMETSÄ, although scandium-bearing columbites were enriched in indium. However, this enrichment is probably due to the indium-iron diadochism again.

Table 3

	Å		Å		Å
Li^{+1}	0·78	In^{+3}	0·92	Cu^{+1}	0·96
Mg^{+2}	0·78			Na^{+1}	0·98
Ni^{+2}	0·78			Lu^{+3}	0·99
Co^{+2}	0·83			Ce^{+4}	1·02
Sc^{+3}	0·83			Yb^{+2}	1·03
Fe^{+2}	0·83			Cd^{+2}	1·03
Zn^{+2}	0·83			Ca^{+2}	1·06
Cu^{+2}	0·83			Y^{+3}	1·06
Hf^{+4}	0·86				
Zr^{+4}	0·87				
Sb^{+3}	0·90				
Mn^{+2}	0·91				

Individual minerals will now be considered, following the sequence of Table 2.

The virtual absence of indium in the graphite samples is to be expected, since indium is too large an atom to replace carbon, and is chemically dissimilar.

Among the oxides analysed here the only indium values are for igneous iron oxides, where the In^{+3}—Fe^{+2} substitution has been operative. Sedimentary oxides will be considered later, but we may note here that HARTLEY and RAMAGE [18] detected indium in such iron oxides, though ERÄMETSÄ did not.

The occurrence of indium in tin and tungsten minerals such as cassiterite, wolframite and scheelite is relevant here. GOLDSCHMIDT [17] reported 0·5 to 10·0 ppm in these minerals, and similar quantities were found by ERÄMETSÄ. PROKOPENKO [32] mentioned indium in cassiterites, as also did BOROVICK and GOTMAN [5]. ITZIKSON and RUSANOV [21] analysed 72 cassiterites from the eastern U.S.S.R., finding from 10–100 ppm in most of them. These last figures are excessively high. AHRENS [2] recently found less than 1·0 ppm indium in a cassiterite from Manitoba, whilst BREWER and BAKER [7] found cassiterites to contain up to 100 ppm. No satisfactory explanation of this association has yet been proposed, and there is no reason apparent to the writer why indium should be enriched in this mineral. BREWER and BAKER, on the other hand, analysed some somplex tin sulphide minerals from a hydrothermal geological environment where indium is known to be commonly concentrated (*q.v.*). Similarly hydrothermal scheelite may contain indium as a result of its chalcophile character. However, it would be interesting to obtain some more accurate indium analyses on cassiterite camples, since AHRENS and LIEBENBERG have recently [3] revived interest in this tin-indium association by showing that samples of mica rich in indium are also rich in tin. Similar work by OTTEMANN [30] showed this Sn—In association, and although his analyses for indium were not quantitative, he was able to show that minerals of several kinds from the Harz which were rich in tin, were also relatively rich in indium. However, OTTEMANN believed that this relation holds only with silicates.

EASTMAN [12] believed that this tin-indium association was due to the nuclear transformation $Sn^{115} \rightarrow In^{115}$. However, there is no evidence of this transformation or that the quantities of tin and indium in minerals are a function of their age (AHRENS and LIEBENBERG [3]). MARTELL and LIBBY [25] have recently shown that

natural decay takes place, but in the opposite direction ($In^{115} \rightarrow Sn^{115}$). However the half-life for this process is $6 \pm 2 \times 10^{14}$ years, and only insignificant quantities of indium have decayed to tin throughout geological time.

Erämetsä established the predominant chalcophile tendencies of indium, showing that in hydrothermal deposits it commonly follows zinc, and sometimes copper. Thus sphalerite samples from numerous Finnish deposits contained up to 1 % In, the average being about 100 ppm. Only two samples out of forty showed less than 1 ppm. The lack of indium in the sphalerite of the present study (S 135) is inexplicable, since this sample comes from Pitkäranta, where there is usually a high indium content. However, the sample analysed was light-coloured, and Erämetsä found these varieties to contain less indium. The large number of sphalerite analyses in his work show that wherever this mineral is forming, it will collect all the indium available. The only other mineral showing a fairly consistent indium enrichment is chalcopyrite, and possibly chalcocite. These associations are in agreement with the figures of Table 3, the replacement of zinc by indium in sphalerite probably being accompanied by an equivalent replacement of zinc by copper (univalent) to balance valencies, as suggested by Erämetsä.

Numerous other authors have detected indium in sphalerite. Hartley and Ramage [18] used an elementary spectrographic procedure which could not have had a very high sensitivity. They detected indium in nine sphalerites, four hematites, four pyrites, one stannite, one chalcopyrite, one magnetite, one manganese ore, and in all five siderites and all four cassiterites analysed. Zakharov and Yushko [44] found 200 ppm in zinc ores from Karpushinsky. Cambi and Maletesta [9] found a Sardinian sphalerite to contain 70 to 120 ppm. Abramov and Rusanov [1] have recorded the presence of indium in sphalerites, as have Szelenyi and Vogl [41]. Stoiber [40] has given a useful review of the literature concerning indium and other trace elements in sphalerite. His own analyses (semi-quantitative) show up to 1 % indium with most analyses in the range 10 to 1000 ppm. A semi-statistical treatment suggests that indium is commonly enriched in mesothermal zinc blende. This conclusion is essentially similar to that reached by Oftedal [29], in a study of Norwegian zinc-blendes. His highest value was 700 ppm.

The absence of indium in halides is to be expected, in view of their crystal structure.

Considering the silicates next, the indium values are rather erratic, but indicate the camouflage or capture of indium by iron. The highest values of all are 5·8 ppm and 4·5 ppm in a hornblende and a mica respectively. This is to be expected, since the In^{+3}—Fe^{+2} replacement necessitates a second or "coupled" replacement to balance valencies, and these minerals have considerable elasticity in this respect. In accordance with this the biotite samples of Ottemann [30] also showed the highest (qualitative) indium contents of all minerals analysed. The kaolin sample (S 18) with a content of 0·12 ppm is a little surprising, but it is conceivable that the indium was adsorbed during sedimentary deposition rather than replacing aluminium in the mineral. The absence of indium in all the feldspar samples is in accord with the improbability that an indium feldspar could exist, as implied by Schiebold [37]. Romeyn [36] reported 1·0 to 2·8 % indium in a pegmatite from Utah, probably replacing aluminium in cordierite. No other details were given, and it would be unwise to accept these high figures without the confirmation of further study. The

rather erratic values among the iron-bearing silicates allows the possibility that "indium provinces" exist, as suggested by Erämetsä. In other words, certain areas of the earth's crust might be richer in indium than others, so that all the minerals in such an area would be proportionately richer in indium. This concept will be discussed later.

The relatively high abundance of indium found by Erämetsä in the niobium-tantalum pegmatite minerals of western Finland led him to the conclusion that indium is to some extent stored up during magmatic crystallisation, being concentrated in pegmatic liquids: this was believed to follow from the greater ionic radius of indium compared to the usual magmatic elements ([13], p. 62). Whilst the present writer acknowledges that Erämetsäs figures suggest an abundance of indium in the residual magma, he cannot accept the above explanation. If indium is present in a magma in which mica or amphibole is crystallising those minerals could easily accommodate the indium, which due to its higher charge would probably replace iron in earlier minerals, although its radius is greater than iron. The indium abundance in the pegmatite minerals might possibly be due to leaching from the wall-rock, as is believed to account for the richness of scandium in certain pegmatite minerals (Goldschmidt [15]), but this needs investigation.

At this point it is convenient to recall the previously mentioned observations of Hartley and Ramage [18] that siderite frequently contains indium. This has been mentioned by Goldschmidt [16], who pointed out that $InBO_3$ is isomorphous with $FeCO_3$ and the exchange Fe^{+2}—In^{+3} is very probably accompanied by the coupled replacement C^{+4}—B^{+3}.

The distribution of indium in minerals may be summarised as follows. Firstly, indium occurs most abundantly in sulphides, associated with Zn^{+2} and Cu^{+1}. Secondly, in common silicates it shows diadochism with Fe^{+2} in mafic minerals. Lastly, other workers have found indium to be enriched in various rare pegmatite minerals usually containing Sn^{+4}, of which the principle one is cassiterite.

Igneous Rocks

In the light of the results from the preceding section, the abundances of indium in igneous rocks will now be considered. For the igneous rocks are composed of silicates and it has been shown that indium replaces iron in mafic silicates. Moreover the valency difference between divalent iron and trivalent indium would tend to strengthen the bonding for the latter element, so that it would be concentrated in high temperature (*i.e.* early) minerals. In the phraseology of Wickman [43],

$$E_{In} > E_{Fe},$$

in six-fold co-ordination. However, it must be remembered also that the radius of indium is greater than iron, which would lead to the opposite conclusion.

$$i.e. \quad \text{that} \quad E_{Fe} < E_{In}.$$

Which of these two effects would be the more important cannot be definitely stated, but it is highly probable that the valency effect would outweigh the latter, thus concentrating indium in earlier silicates.

Goldschmidt and Hörmann (Goldschmidt [17]) found indium concentrations of 0·5 to 1·0 ppm in the early pyroxene-rich basic rocks and these observations

are in accord with the above arguments. However when we turn to the results of the present work and of other workers, the position seems more complicated.

Thus in Table 2 there are a number of basic and ultra basic rocks, but although several of them are pyroxene rich (*e.g.* S 143, 21, 24, 23, 71, 90, 112, 113, 61, 137, 140, 141, 138), they have very variable indium contents, ranging from virtually zero to 0·32 ppm. Similarly the hornblende-bearing rocks (S 63, 142) are by no means indium-rich. All these rocks are comparatively rich in iron and are of early crystallization. The mean indium contents in basalt and gabbro are 0·22 and 0·015 ppm respectively. These figures are in fairly good agreement with previous values reported by Preuss [31] and Borovick, Prokopenko and Pokrovskaya [6], as listed in Table 4.

The intermediate igneous rocks seem uniformly poor in indium and the same holds true of the silicic rocks, with one or two exceptions. Thus out of fourteen high-silica rocks only three show indium-values, yet the 2·0 ppm in the Bomarsund granite (S 55) is the highest of all the igneous rocks, and makes the mean value for the ten granites 0·26 ppm. This average value is greater than those for the basic rocks, but the individual figures show that indium does not become enriched in granitic rocks, but rather the opposite is the case. In Table 4 are presented some earlier figures for comparison. Borovick, Prokopenko and Pokrovskaya [6] and Prokopenko [32] found the same variable indium contents of granites, their figures ranging up to 1·9 ppm. On the other hand Preuss [31] found a definite indium enrichment in German granites, as is evident from the high average of 2·0 ppm.

Consequently, the distribution of indium in igneous rocks seems to be very haphazard. Basic rocks frequently contain appreciable indium, but the highest individual values occur in the granites. This does not appear to be in accordance with crystal chemical considerations, if indium is camouflaged in the silicates, but there are two possibilities which could reasonably explain these facts. Either the indium is present in the silicates and there exist indium provinces in time or space, or else the indium is contained partly or wholly in some other mineral. In the first case, it would be reasonable to expect a high value in a sample from a region of the crust rich in indium, even in a rock normally impoverished in that element. Such a view is held by Erämetsä, who believes that the Pitkäranta region in K.F.S.S.R. constitutes an indium province. However, an examination of the distribution of the igneous samples in the present work, and their ages, gives no suggestion at all of such provinces. Even the fact that most of the indium figures are Finnish rocks only reflects on the preponderance of such rocks analysed.

It is concluded that there is no evidence in the present analyses suggesting the existence of large-scale indium provinces. This of course does not deny their existence on a smaller scale which can be revealed by comparative analyses over limited areas.

The second possibility seems more likely. Apart from the silicates all igneous rocks contain varying amounts of iron oxides and of sulphides. The former undoubtedly carry a little indium, as shown by the analyses of two such separated oxides (S 116 and 154) containing 0·071 and 0·12 ppm. However the iron oxides seldom constitute more than 5% of an igneous rock and can contribute little to the whole analysis. On the other hand, the sulphides are usually present in much smaller

quantities. The normal magmatic accessory sulphides are pyrite, pyrrhotite and chalcopyrite, and of these chalcopyrite probably contributes most significantly to the indium content. However ERÄMETSÄ has shown that this mineral can contain up to 1000 ppm and in rare instances a small quantity of sulphide may notably increase the whole indium content. If some hydrothermal sulphides were introduced also, perhaps containing a little sphalerite, the indium content might well be much higher. Sphalerite is not unknown in igneous rocks, but is probably never of primary origin.

The above hypothesis would be well worth investigating. A rock showing a surprisingly high indium content, such as the Bomarsund granite, could be separated into its constituent phases and these analysed to find where the indium is located. A great deal more factual knowledge is required in any case, before the two possibilities outlined above can be profitably discussed in any detail. For the present we must recognise an anomaly in the distribution of indium in igneous rocks.

In Table 4 the average for each rock type has been calculated, in spite of the previous remarks, and figures from other authors presented for comparison.

Table 4. Indium in igneous rocks

Rock type	*Number of samples*	*Average* In *ppm*	*Reference*
Anorthosite	2	—*	
Peridotite and Pyroxenite	4	0·013	
Basalt	4	0·22	
Gabbro	6	0·015	
Diorite and Andesite	2	—*	
Syenite and Monzonite	3	—*	
Granodiorite etc.	4	—*	
Granite	10	0·26	
Rhyolite Obsidian	2	—*	
Nepheline Rocks	3	—*	
Basic Pyroxene-rich rocks	—	0·5–1·0	GOLDSCHMIDT [17]
Composite of 11 German Gabbros	—	0·3	PREUSS [31]
Composite of 14 German Granites	—	2·0	PREUSS [31]
Composite of 8 Russian Gabbros	—	—*	BOROVICK, PROKOPENKO and POKROVSKAYA [6]
Composite of 12 Russian Granites	—	0·05	BOROVICK, PROKOPENKO and POKROVSKAYA [6]
Nepheline syenite	1	0·09	BOROVICK, PROKOPENKO and POKROVSKAYA [6]
Monzonite	1	1·9	PROKOPENKO [32]

* Too low to measure.

SEDIMENTARY ROCKS

There are very few quantitative data regarding the distribution of indium in sediments, and the discussion will therefore be concerned almost entirely with the analyses under this heading in Table 2. Fortunately the content is appreciable in most of these.

The sedimentary deposits are composed in part of rock detritus, in part of amorphous chemical deposits and in part of crystalline chemical deposits. Trace

elements may of course be present in all three of these materials, and in the first and the last they will be camouflaged within minerals in the usual way. The amorphous materials are chiefly colloidal, and whether a given trace element occurs in this type of environment depends to a large extent on surface chemistry. Elements which are not incorporated in sediments in any of these three ways may still be deposited as a result of biological activity, when for example an organism takes the element in as a nutrient and later dies, its remains contributing to sedimentary deposition.

As in other geochemical processes, an element can only be incorporated in a sediment when there is an initial supply. This comes in the main from the weathering of other rocks, though for some elements volcanic emanations are of great importance. Present-day erosion affects all varieties of rocks, but at the beginning of geological time there was only igneous rock to be croded. Thus the erosional constituents of all sedimentary rocks came originally from igneous rocks. In the following discussion we shall to some extent ignore the detrital materials, since they simply represent fragments of igneous and other rocks and afford no new principles. Rock weathering takes place by physical and chemical processes, the latter taking place in aqueous solution. As a result of the chemical breakdown of minerals, their constituent elements either go into true solution, or are carried in a colloidal suspension. Under suitable conditions a given element may be partially or wholly precipitated, being thereby incorporated into sediments as mentioned above. If precipitation does not occur, the element will either be removed by organic processes or will be carried down to the sea.

If we consider the behaviour of indium during sedimentation processes the first relevant data concerns its oxidation state after weathering from rocks. Weathering is essentially a process of oxidation, and iron is usually converted to the ferric state giving the familiar red colour of many sedimentary rocks. The redox potential of the reaction

$$Fe^{+2} = Fe^{+3} + e$$

is 0·77 v (25° C; $p_H = 0$). Thus the oxidising environment of ordinary weathering maintains this potential (modified for p_H and temperature changes). Of the various oxidation-reduction couples for indium in different states the highest redox potential is 0·45 v, for the reaction

$$In^{+2} = In^{+3} + e \quad \text{(Latimer [23])}.$$

This implies that in ordinary weathering indium remains in the trivalent state.

The solubility behaviour of any element depends on its ionic potential (quotient of ionic charge and radius) as has been demonstrated by Goldschmidt [16]. Elements of intermediate ionic potential—usually between 3·0 and 10·0—are hydrolysed and precipitated from solution. Such elements include aluminium and iron, and trivalent indium with an ionic potential of 3·3.

The above considerations are substantiated by the analyses of sedimentary rocks in Table 2. The absence of indium in the detrital sandsones is expected, in view of the previously demonstrated absence in their constituent minerals, quartz and feldspar. The bauxite (S 171) is a residual deposit seen to be slightly enriched in indium, reflecting the influence of ionic potential. Similarly, most of the argillaceous rocks show varying indium values, consistent with accumulation due to hydrolysis. It might be noted in passing that the properties, solubility and amphoteric character

of indium hydroxide are closely similar to aluminium hydroxide, and the hydrolysis has been studied experimentally (see MELLOR [26] p. 398). The average of the argillaceous sediments (including present-day marine samples) is 0·054 ppm which is only a tenth of PREUSS' [31] average for German shales. However BOROVICK, PROKOPENKO and POKROVSKAYA [6] were unable to measure the indium content of a composite of sixteen Russian clays, which therefore presumably contained less than perhaps 0·05 ppm (in view of their other figures), and they also found that indium was absent in twenty different present-day muds. In other clays however, they state that up to 10 ppm were present. The slate from Crystal Falls, Michigan (S 174) is the matrix material surrounding the pyrite (S 173). The absence of indium in the pyrite, which is authigenic, and the small but appreciable value in the slate is rather surprising after the chalcophile tendencies of indium have been discussed. Perhaps at the low temperature of authigenic growth pyrite is intolerant of large foreign ions.

The enrichment of indium in the Dictyonema shale and the anthraxolite (S 117, 151), is interesting, and may be due to organic enrichment processes. There is, however, no enrichment in the other organogenic sediments of this kind (S 66, 67, 68, 153) though the low figure for the pure graphite (S 69) may be recalled. The absence of indium in the anthracite (S 153) is to be expected, since the analysis was not performed on the ash.

GOLDSCHMIDT [16] has mentioned the presence of indium in marine phosphates, where it presumably replaces iron. Also, as mentioned previously, indium replaces iron in some carbonates. Neither of these processes is apparent in the present work, with reference to the phosphorite-glauconite sandstone (S 91) and the carbonate samples S 64 and 65.

The virtual absence of indium from the manganese-iron rich sediments (S 103, 105, 17, 19, 170) is also in contradiction to GOLDSCHMIDTs [17] statement that indium follows iron and manganese in sedimentary rocks. This is difficult to understand, since iron and indium have rather similar ionic potentials, and an oxidising environment strong enough to precipitate iron would also precipitate indium.

The deep sea samples in Table 2 have no special features requiring comment, beyond the fact that indium is absent from the oozes (S 106 and 109), due to the diluting effect of the carbonate and silica skeletons mixed with the clay material. The average figures for different sediment types are summarised in Table 5.

Table 5. Indium in sediments

Rock type	*Number of samples*	*Average* In *ppm*	*Reference*
Argillaceous	16	0·054	
Arenaceous	3	—*	
36 German shales		0·5	PREUSS [31]
23 German sandstones		0·3	PREUSS [31]
16 Russian clays		—*	BOROVICK, PROKOPENKO and POKROVSKAYA [6]

* Too low to measure.

Metamorphic Rocks

Very little is known about the geochemical changes accompanying metamorphism, but the previous work on thallium, (Shaw [38]), suggested a definite behaviour pattern for that element. With indium there is no such regular behaviour, as might be anticipated from earlier discussion. Table 2 contains the analyses of three sets of metamorphic rocks, from Wyoming, Greenland and New York State.

The first group of rocks is believed to constitute a related group having originated by metasomatic replacement of pre-existing rocks, (W. H. Newhouse, A. F. Hagner and G. de Vore, unpublished work). There appears to be no consistency in the few indium analyses obtained.

The samples from Greenland and from New York consist of two groups of rocks of roughly the same composition but in different grades of metamorphism. Thus the Greenland rocks are quartzo-feldspathic gneisses, of which samples S 110 and 111 are in the amphibolite facies and the other four in the granulite facies. The Dutchess county rocks from New York (Balk and Barth [4]) are samples of argillaceous sediments at different metamorphic grades. It would be profitless to discuss these rocks at length, since the indium contents seem quite irregular, the only feature of note being that the highest values in each case are in rocks carrying garnet and mica.

Miscellaneous Samples

The apparent absence of indium in the three meteorites analysed is rather surprising, because Hörmann (in Goldschmidt [17]) found 1·0 ppm in a troilite and in an iron meteorite, and Goldschmidt (*ibid*) suggested 0·15 ppm. In as an average for all meteorites.

Due to arcing difficulties, the sensitivity limit for the ocean salts cannot be as low as with the silicates, but is perhaps 0·6 ppm. This would correspond to a concentration of 0·02 ppm in ocean water. No figures are available for the indium content of ocean water, but it must be very low.

Crustal Abundance of Indium

In the preceding work on thallium (Shaw [38], consideration was given to the problem of computing a crustal abundance, and it is unnecessary to repeat the discussion here.

In the case of indium it is debatable whether there is any value in a terrestrial abundance figure. For the igneous rocks have exceedingly erratic values, which are not confined to the present study moreover. However, the computation has been carried out, and is presented in Table 6. Here the method of Knopf [22] has been used. From forty-six of the igneous rocks in Table 2 the averages have been calculated. Each is multiplied by the appropriate abundance factor (certain of Knopf's minor rock types have been grouped together). The sum of the products expresses the mean terrestrial abundance, with an analytical error of $\pm 20\%$.

It is of interest to note that if the simple average of all the igneous rocks had been calculated, a figure of 0·09 ppm would have been obtained. The difference is about 20%, which is within the experimental error of the present work, but would be a serious difference in a study of higher precision.

Table 6. Indium content of the mean igneous rock

Rock type	*Number of samples*	In *mean ppm*	*Abundance factor*	*Weighted* In *mean ppm*
Diorite and Andesite	2	—	0·255	—
Granite	10	0·26	0·230	0·060
Basalt	4	0·22	0·206	0·045
Rhyolite Obsidian	2	—	0·127	—
Granodiorite etc.	4	—	0·126	—
Gabbro	6	0·015	0·038	0·000
Syenite and Monzonite	3	—	0·008	—
Peridotite and Pyroxenite	4	0·013	0·004	0·000
Anorthosite	2	—	0·003	—
Nepheline Rocks	3	—	0·001	—
			Total:	0·105

Mean crustal abundance of Indium $0{\cdot}11 \pm 0{\cdot}02$ ppm.

To aid in consideration of this result Table 7 has been compiled, giving abundance figures according to earlier workers.

Table 7

Reference	*Crustal abundance of indium ppm*
F. W. Clarke and H. S. Washington [10]	0·01–0·10
I. and W. Noddack [27]	0·1
I. and W. Noddack [28]	0·016
V. M. Goldschmidt [17]	0·1
E. Preuss [31]	0·3 2·0
N. M. Prokopenko [32]	0·05 (Russian granites)
Present results	0·11

With reference to Preuss' work, the two figures express his indium analyses of gabbros and granites respectively, but no abundance figures were stated explicitly. Prokopenko likewise made no such calculation, and his figure for Russian granites is inserted for comparison only.

On comparing the figures in Table 7 the most surprising feature is their general agreement, bearing in mind that much of the earlier work was semi-quantitative only, and also bearing in mind the erratic distribution of indium. The high figures of Preuss have already been discussed in a previous section. Otherwise there is rather close agreement of the previous values with the new figure. The new figure therefore may be accepted provisionally, but it must be regarded as a lower limit, since a more sensitive analytical method would have detected indium in the numerous samples for which no figures were obtained. Moreover the possible existence of indium provinces, suggested by Eräметsä, needs further investigation and might prove a significant factor in this respect.

General Geochemistry and Major Cycle of Indium

It has been a useful hypothesis for over a century that meteorites are particles from a disintegrated planet of similar nature to the earth. Recent work by Brown and Patterson [8] has shown that this is consistent with thermo-dynamic interpretation of the chemistry of meteorites. Accordingly, it is perhaps permissible to take Goldschmidts [17] suggested figure of 0·15 ppm, representing the average indium content of all meteorites, as being a first approximation to the indium content of the whole earth. This figure cannot be regarded as being at all precise, however, and is probably too high, since no indium could be detected in meteorites in the present work. Nevertheless it suggests that the abundance in the crust of the earth is similar to that for the earth as a whole or, in other words the primordial earth differentiation does not appear to have given rise to a pronounced indium enrichment at the surface of the earth.

To find the theoretical reasons for this behaviour some thermochemical figures must be reviewed in the light of probable earth composition. If we assume that the earth consists of a metallic core surrounded by silicate shells, then every element will be present in both these materials. For the earth must have consisted at one time of two immiscible liquid phases, one metallic and one magmatic, and each element was distributed across these two phases. Which phase it was concentrated in depends on its affinity for oxygen, measured by the free energy of formation of the oxide. An element whose oxide had a greater free energy than ferrous oxide would be preferentially concentrated in the magmatic liquid, and vice-versa. Strictly speaking the quantities involved should be the free energies of silicates, but these are not known, and the oxides are believed to be sufficiently similar in this respect to serve in their stead. In Table 8 are presented some free energies of relevant oxides, expressed in kilogram-calories per gram atom of oxygen (Rankama and Sahama [35] Table 4.4).

Table 8

Oxide	$-\Delta F_0$
Na_2O	93·6
In_2O_3	72·7
FeO	59·3
Cu_2O	35·1

Thus sodium, with a free energy formation of the oxide considerably greater than iron, is strongly concentrated in the silicate melt and impoverished in the metallic phase, whilst with copper the reverse is true. The position of indium is not so clear, owing to uncertainty regarding the figure in the above table*. Assuming however that this figure is correct, the behaviour of indium might be expected to be rather similar to iron with however a slight tendency for enrichment in the silicate shell. This is in good agreement with the figures above, and suggests more strongly that Goldschmidts [17] figure of 0·15 ppm as an average for all meteorites (and hence the earth) is somewhat too high.

The previous arguments have of course ignored the fact that whenever a liquid sulphide phase is present we have every reason to believe that indium will be concentrated there to a far greater degree than in either of the other liquid phases.

Indium therefore should be present in silicate magmas to a small extent, and as has been discussed above, will be incorporated in iron silicates during crystallisation.

*The correct value for $-\Delta F_0$ for In_2O_3 appears to be $3 \times 72{\cdot}7$ or 218 kg-cals (Latimer [23] p. 150). However Latimer (*ibid* p. 304) quotes a value of 21·8, which is adopted in several standard chemical reference books.

due to replacement of Fe^{+2} by In^{+3}. Although the cafemic igneous rocks on this account should show an indium enrichment compared with alkali-silicic rocks, this behaviour is not very evident and there is a rather erratic distribution. It has been suggested that this might be due either to an initial enrichment of certain magmas (*i.e.* indium provinces), or alternatively the indium may be present in accessory sulphides formed under hydrothermal conditions. Certain pegmatite minerals, usually complex oxides, are said to be enriched in indium, and the causes of this are obscure. It is especially difficult to explain the occurrence of indium in cassiterite. Hydrothermal deposits are often enriched in indium, which is commonly present in the zinc and copper sulphides, as well as in the rare complex tin sulphides. Sphalerite is the common source of indium, and concentrations up to 1% In have been frequently reported. No true indium minerals exist.

The mean igneous rock contains 0·11 ppm indium. During weathering indium is commonly transported towards the sea, probably as a colloidal hydroxide suspension. Other authors have observed the tendency for indium to be precipitated along with iron and manganese oxides, but the present author and Eräметsä [13] found no evidence for this. The indium appears ro remain in suspension until flocculation takes place when the sea is reached, the precipitated material being incorporated in argillaceous sediments. Some indium must remain in solution in sea water, since it has been found in marine phosphates of chemical (and possibly biological) origin, but the quantity in solution is too minute to detect. In addition to the indium accounted for in this way there is some evidence that indium is concentrated slightly by other biological factors, since a slightly increased concentration has been noted in some carbonaceous shales, and Goldschmidt [16] has reported up to 2·0 ppm in coal ash. This may probably be attributed to the establishment of a strong reducing environment during the bacterial reduction of dead organic matter, and the consequent incorporation of indium in authigenic sulphides.

Goldschmidt [14] has considered in detail the quantitative aspects of sedimentation, with a view to finding the "fate" of elements released during weathering. It is not profitable to set up equations to account for the distribution of indium during sedimentation, on account of the uncertainty and unreliability of the average figures computed in this work. However, if we note that 160 kg of mean igneous rock containing 0·11 ppm indium is weathered to give about 155 kg of clay and sandstone sediments, where the mean indium content of argillaceous deposits is 0·054 ppm, we see that about half the indium is unaccounted for, since the figure for arenaceous rocks must be very low. It seems, most probable that this missing indium, has probably been concentrated in other hydrolysate sediments not accounted for in the usual calculations. Thus the bauxite deposits and possibly even the sedimentary iron ores are quantitatively insignificant, but may contain sufficient indium to account for the balance. It is not likely that the indium is present in limestones and dolomites however, to any noteworthy extent.

In conclusion, it will be apparent that although a reasonably coherent framework has been set up to delineate the main features of indium geochemistry, there still remain numerous and important lacunae which need investigation. Work on the apparent association of indium and tin will be continued in this laboratory.

References

[1] Abramov, F. I. and Rusanov, A. K.; Soviet Geol. 1938 **8** (No. 5) 64–73. [2] Ahrens, L. H.; Nature, Lond. 1948 **162** 313. [3] Ahrens, L. H. and Liebenberg, W. R.; Amer. Mineral. 1950 **35** 571–578. [4] Balk, R. and Barth, T. F. W.; Bull. Geol. Soc. Amer. 1936 **47** 685–850. [5] Borovick, S. A. and Gotman, J. D.; Compt. rend. (Doklady) acad. sci. U.R.S.S. 1939 **23** 351–354. [6] Borovick, S. A., Prokopenko, N. M. and Pokrovskaya, T. L.; Compt. rend. (Doklady) acad. sci. U.R.S.S. 1939 **25** 618–621. [7] Brewer, F. M. and Baker, E.; J. Chem. Soc. for 1936, 1286–1290. [8] Brown, H. and Patterson, C.; J. Geol. 1948 **56** 85–111. [9] Cambi, L. and Maletesta, L.; Rend. inst. lombardo sci. 1936 **69** 369–374. [10] Clarke, F. W. and Washington, H. S.; U.S. Geol. Survey Profess. Paper 127. 1924. [11] Daly, R. A.; Igneous rocks and their origin. McGraw-Hill, New York 1914. [12] Eastman, E. D.; Phys. Rev. 1937 **52** 1226–1227. [13] Erämetsä, O.; Ann. Acad. Sci. Fennicae, Ser. A. 1938 **50** (No. 1). [14] Goldschmidt, V. M.; Fortschr. Mineral. Krist. Petrog. 1933 **17** 112–156. [15] Goldschmidt, V. M.; Geol. Fören. Stockholm Förh. 1934 **56** 385. [16] Goldschmidt, V. M.; J. Chem. Soc. for 1937 655–673. [17] Goldschmidt, V. M.; Skr. Norske Vid.-Akad. Oslo, 1937, 1. Mat.-naturv. Klasse, No. 4. [18] Hartley, W. N. and Ramage, H.; J. Chem. Soc. 1897 **71** 533–550. [19] Hasler, M. F. and Kemp, J. W.; J. Opt. Soc. Amer. 1944 **34** 21–32. [20] Honerjäger-Sohm, M. and Kaiser, H.; Spectrochim. Acta 1944 **2** 396–416. [21] Itzikson, M. I. and Rusanov, A. K.; Compt. rend. (Doklady) acad. sci. U.R.S.S. 1946 **53** 631–632. [22] Knopf, A.; J. Geol. 1916 **24** 620–622. [23] Latimer, W. M.; The oxidation states of the elements and their potentials in aqueous solution. Prentice-Hall Inc. 1938. [24] Ludwick, M. T.; Indium. Indium Corporation of America, 1950. [25] Martell, E. A. and Libby, W. F.; Phys. Rev. 1950 **80** 977–982. [26] Mellor, J. W.; A comprehensive treatise on inorganic and theoretical chemistry, Vol. V., Longmans, Green and Co, London 1924. [27] Noddack, I. and Noddack, W.; Naturwiss. 1930 **18** 757. [28] Noddack, I. and Noddack, W.; Svensk Kem. Tid. 1934 **46** 173–200. [29] Oftedal, I.; Skr. Norske Vid.-Akad. Oslo, 1940 1. Mat.-naturv. Klasse, No. 8. [30] Ottemann, J.; Z. angew. Mineral. 1940 **3** 142–169. [31] Preuss, E.; Z. angew. Mineral. 1940 **3** 8–20. [32] Prokopenko, N. M.; Compt. rend. (Doklady) acad. sci. U.R.S.S. 1941 **31** 903–906. [33] Rankama, K.; Bull Comm. géol. Finlande 1944 (No. 133). [34] Rankama, K.; Ann. Acad. Sci. Fennicae, Ser. A. 1948 **3** 13. [35] Rankama, K. and Sahama, Th. G.; Geochemistry. Chicago 1950. [36] Romeyn, H.; J. Amer. Chem. Soc. 1933 **55** 3899–3900. [37] Schiebold, E.; Fortschr. Mineral. Krist. Petrog. 1932 **16** 111–112. [38] Shaw, D. M.; Geochim. et Cosmochim. Acta 1952 **2** 118. [39] Shaw, D. M., Joensuu, O. I. and Ahrens, L. H.; Spectrochim. Acta 1950 **4** 233–236. [40] Stoiber, R. E.; Econ. Geol. 1940 **35** 501–519. [41] Szelenyi, T. and Vogl, M.; Magyar Kir. Foldt. Intezet Erkönyve 1941 **35** 61–67. [42] Vernadsky, W.; La géochimie. Paris, 1924. [43] Wickman, F. E.; Geol. Fören. Stockholm Förh. 1943 **65** 371–396. [44] Zakharov, E. E. and Yushko, S. A.; Tr. All-Union Sci. Research Inst. of Econ. Mineral., 1935, Fasc. 75.

Geochimica et Cosmochimica Acta, 1952, Vol. 2, pp. 207 to 210. Pergamon Press Ltd., London

A preliminary investigation into the isotopic composition of carbon from some alkaline intrusions[1]

H. von Eckermann*, H. von Ubisch** and Frans E. Wickman***

(Received 6 November 1951)

ABSTRACT

Twelve samples of carbonate rocks from Alnö (Sweden), eight samples from Fen, two from Stjernöy and one from Seiland (Norway), have been investigated. The beforsites from Alnö show a lower C^{12}/C^{13} ratio than the soevites and the alvikites from the same area. In the Fen area there is a difference between the iron-rich and iron-poor rocks. The C^{12}/C^{13} ratios of the soevites from all four occurrences are quite consistent. Various factors which might influence the ratio are mentioned.

Introduction

In 1948 one of the authors (H. v. Eckermann [3]) published a new monographic description of the geology of the Alnö alkaline area, showing its formation to be quite complex. In order to see whether such a complex deposit is homogeneous or not with respect to the isotopic composition of carbon, we investigated in 1949 twelve samples representing several rock types selected from various parts of the area. The results obtained were so interesting that we thought it advisable to make a comparison with rock samples from Fen and other Norwegian occurrences which show some similarities and some characteristic differences to Alnö. Through the generosity of our Norwegian colleagues, Prof. Tom. F. W. Barth, Dr. H. Björlykke and Dr. E. Saether, we obtained a series of samples. Recently P. Baertschi [1] published a letter in "Nature" in which he states that he has analysed a number of specimens from some alkaline intrusions. However, no details are given, and therefore we cannot draw any comparisons from his results.

The Geology of the Investigated Areas

The Alnö alkaline intrusion, near Sundsvall in northern Sweden, is of Late Jotnian or post-Jotnian age and is characterized by the occurrence of large deposits of limestone and dolomite. Recent investigations by one of us (H. v. Eckermann [3]) have shown that the Alnö area may be described as formed by a series of consecutive explosions from three foci (Fig. 1) at about 1 km (soevite), 2 km (alvikite) and 7 km (beforsite) below the present outcropping erosion surface. The explosions gave rise to a fracturing of the surrounding and superimposed consolidated rocks and formed cone sheets, ring-dikes and radial dikes.

Simultaneously with the intrusions, fenitisation of the surrounding rocks took place. Mineralogically, soevite and alvikite consist mainly of calcite, and beforsite of dolomite. Alvikite is the dike-rock of soevite, and beforsite is the dike-rock of a rauhaugite poor in iron. Rauhaugite is not represented in the area, however.

[1] Paper No. 4 in a series devoted to the application of isotope ratios to geological problems.

* Sparreholm, Sweden.

** Karolinska Institutet, Stockholm, Sweden.

*** Riksmuseet, Stockholm, Sweden.

Among the samples, all three rock-types are represented and the samples were selected with the view to represent various depths and various chemical compositions of the intrusive carbonate.

The Fen area, near Ulefoss in southern Norway, has undergone change in recent years. According to Saether [5] a primary basic magma, originally rich in carbonates, gives rise on solidifying to a residual magma exceedingly rich in carbonates and produces ultimately carbonatitic alkaline hydrothermal liquids.

Accordingly, some soevite is taken to be magmatic, but the major part is considered to derive from hydrothermal metasomatic metamorphism of basic silicious rocks. A similar genesis is ascribed to the rauhaugite

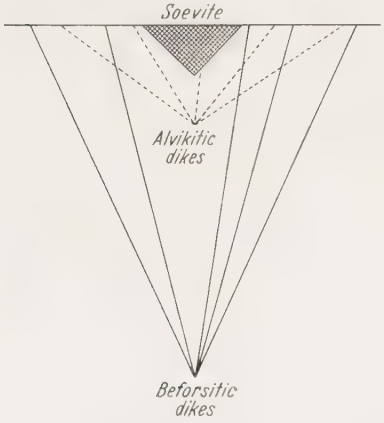

Fig. 1. Schematic section through the Alnö alkaline area.

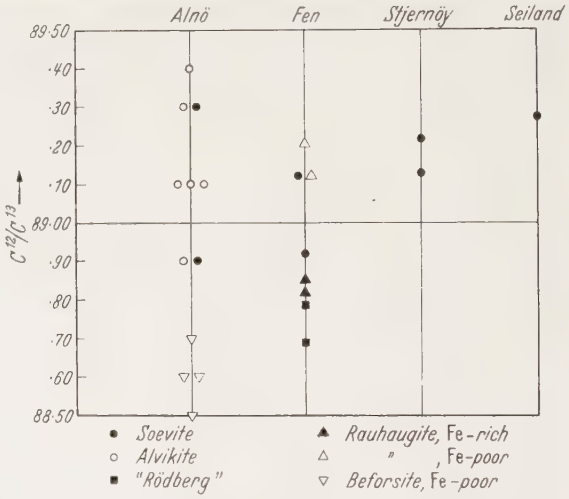

Fig. 2. Diagram showing the distribution of the isotope ratios.

(consisting mainly of dolomite and ankerite) and to the "rödberg" (consisting of calcite, ankerite and exceedingly fine-grained Fe_2O_3). The precipitation of the iron oxide is supposed to have been caused by a drop in pressure following upon an escape of CO_2.

The Stjernöy deposit has not yet been described, but the occurrence of limestones on Stjernöy island is mentioned briefly by Barth [2].

The Seiland area has been described by Barth [2] and according to him the albite-soevite, termed albite-ringite by him, belongs to Caledonian intrusive rocks. The calcite, although magmatically crystallized, is assumed to have been incorporated into the magma by assimilation of calcareous sediments.

Discussion

The samples were prepared for analysis as described in another paper [6]. The analyses of the Alnö samples were made by H. v. Ubisch in 1949 with an old-type mass spectrometer equipped with a single collector. The other samples were analysed in 1951 by Mr. Ryhage using a new double-collector mass spectrometer which gives increased accuracy. The results are given in Table 1. For Alnö the accuracy is within 0·3 unit and for the other samples within 0·1 unit. All samples refer to our standard sample [6].

Table 1

No.	*Name of rock, Locality*	C^{12}/C^{13}
	Alnö area	
1	Soevite, Point W of Hörningsholm, Alnö	89·3
2	Soevite, Drillhole No. 2, Hörningsholm Island, at 100 m depth	88·9
3	Alvikite, Cone Sheet, S *e* in Norrberg *e*	89·1
4	Alvikitic carbonatite, Radial dike, Rödö	89·4
5	Alvikitic carbonatite, Dike No. 5, road cutting, Skönvik	88·9
6	Alvikite, Northern point, Grönviken, Alnö	89·1
7	Alvikite, Eastern point, Långörsholmen	89·3
8	Alvikite, Dike No. 3, road cutting, Skönvik	89·1
9	Beforsite, North-Eastern shore, Fläschön	88·7
10	Carbonatite (beforsite), W of Nacka	88·6
11	Beforsitiic alnöite, Stavreviken	88·6
12	Beforsite dike, Bergeforsen	88·5
	Fen area	
13	Soevite, "Hydrogangen"	89·12
14	Soevite, Tufte	88·91
15	Rauhaugite, poor in Fe, $Dol_{90}Ank_{10}$, Dike in road cutting, Ringsevja	89·21
16	Rauhaugite, poor in Fe	89·12
17	Rauhaugite, rich in Fe, $Dol_{70}Ank_{30}$, Beach W of Fen iron mine	88·85
18	Rauhaugite, rich in Fe, Beach W of Fen iron mine	88·82
19	"Rödberg," Fen iron mine	88·69
20	"Rödberg," Small occurrence between Söve and Norsjö	88·79
	Stjernöy	
21	Soevite, E of Lake Gammevann, Fjellfinndalen	89·12
22	Coarse grained calcite-rich band in soevite, Brook East of Gammevann, Fjellfinndalen	89·21
	Seiland	
23	Albite-soevite (albite-ringite)	89·27

The results are plotted in a diagram (Fig. 2), and it is obvious from the figure that the soevites and alvikites from Alnö show the same range of variation. On the other hand, the beforsites show a somewhat different distribution, giving slightly lower values of the C^{12}/C^{13} ratio. As these twelve samples were given to the operator in random order and marked only with numbers, it is most unlikely that this difference in the distribution is insignificant. So it may be taken for granted that those rocks that derive from the deeper focus are enriched in the heavy isotope. One of us (H. v. ECKERMANN) has previously suggested ([3] p. 153) that cation exchange between the dolomitic magma and the wall rocks, as well as TP-instability, led to a gradual decomposition of the dolomitic carbonate and to an ultimate accumulation of soevite and carbon dioxide at the upper focus. In consequence, the carbon dioxide, liberated during the metasomatism, may have been enriched in the light isotope.

This confirms the deduction previously drawn by one of us (F. WICKMAN [6]) that cation metasomatism gives an enrichment of the heavy carbon isotope, this being the case during the formation of the beforsites.

In Fen the soevite specimens show the same values as the Alnö specimens, but the rauhaugite, which is unknown in the Alnö area, shows a very interesting distribution. The members poor in iron are enriched in C^{12} compared to the iron-rich samples. Until Saethers final report on Fen has appeared, any attempt at explaining this may be premature.

The samples from Seiland and Stjernöy give the same values as the specimens of soevite from Alnö.

The work has been financially supported by a grant from *Staleas Naturvetenskapliga Forskningsråd.*

References

[1] Baertschi, P.; Relative abundance of oxygen and carbon isotopes in carbonate rocks. Nature, Lond. 1951 **168** 288–289. [2] Barth, T.; Die Pegmatitgänge der kaledonischen Intrusivgesteine im Seiland-Gebiete. Skrifter. Norske Videnskap-Akademi Oslo. I Mat.-Naturv. Kl. No. 8, 1927. [3] Eckermann, H. v.; The alkaline district of Alnö Island (Alnö alkalina område). Sveriges Geol. Unders. Ser Ca No. 36, 1938. [4] Mars, K. E.; A preliminary investigation of the relative abundance of the carbon isotopes in Swedish rocks. J. Geol. 1951 **59** 131–141. [5] Saether, E.; Foreløpig meddelse om resultatet av undersøkelser i Fensfeltet. Norsk Geol. Tidskr. 1949 **27** 66–73. [6] Wickman, F. E., Blix, R. and Ubisch, H. v.; On the variations in the relative abundance of the carbon isotopes in carbonate minerals. J. Geol. 1951 **59** 142–150.

I. General

1. Papers on Geochemistry should be submitted to the editors for the appropriate country or language (*Papers on Cosmochemistry should be sent Prof. F. A. Paneth, F.R.S.*). Papers submitted for publication will naturally be judged from the standpoint of scientific originality and novelty. Technical details of apparatus used in scientific investigation can, however, be presented in brief notes. The preparation of progress reports and review articles will be invited by the Editors from time to time and it is therefore requested that no uninvited contributions of this nature be submitted. The Journal will appear as independent and complete numbers, which will be sold separately and combined into volumes of about 300 pages.

2. Only papers which have not been previously published will be accepted. The publishers retain exclusive publication rights for all papers in all languages and countries, on acceptance an until the 31st December of the year following the year when the printed paper appears. Authors must agree not to publish elsewhere a paper submitted to and accepted by *Geochimica et Cosmochimica Acta.*

3. Authors will receive 75 free reprints of their papers. Additional copies can be purchased if ordered at the time the first proofs are returned.

II. Manuscript Requirements

1. The manuscript must be written in one of the three official languages, English, French, or German.

2. The manuscript should be an original typewritten copy (not a carbon). The text must be ready for printing and should be carefully checked for errors. Authors will receive proofs for correction.

3. Half-tone illustrations are to be restricted to the minimum necessary. They must accompany the manuscript mounted on separate sheets. Line drawings will be redrawn for the sake of uniformity and should therefore include all relevant details. Photographs should be enlarged sufficiently to permit their clear reproduction in half-tone. If words or numbers appear in photographs, two copies are requested, one clearly printed and the other without inscription. All illustrations and tables should be provided with descriptive legends.

4. Only such references to literature should be given as are referred to in the text. Literature references are to be numbered and listed together at the end of the manuscript and not as footnotes All references should include the standard (according to the *World List of Scientific Periodicals*) abbreviated title of the journal, year, volume number, and first and last page numbers.

5. The text of articles submitted should be concise and in a readily understandable style. The technical description of the methods used should only be given in detail when such methods are new. The essential contents of each paper should be briefly recapitulated in an abstract in English. Such an abstract may, however, be submitted by the author in the language of the original typescript for translation into English by the editorial staff.

6. To conserve space authors are requested to mark less important portions of the paper (such as description of methods, record of experimental results, *etc.*) for printing in smaller size type.

The Unesco Book Coupon Scheme

Under a scheme initiated by the United Nations Educational, Scientific and Cultural Organization, Book Coupons can now be purchased in national currency for the purpose of obtaining publications of a scientific, educational and cultural nature from other parts of the world.

Coupons are available in various denominations at distributing agencies in the following countries:— Burma; Czechoslovakia; Egypt; France; Hungary; India; Indonesia; Israel; Italy; Pakistan; Persia; Thailand; Union of South Africa; at UNESCO Science Co-operation Offices in East Asia, the Middle East and South Asia; and for British, Colonial and Trust Territories from Book Tokens Ltd., 28 Little Russell Street, London, W.C.1.

Since the amount of coupons available is sometimes limited, special priority is given to the needs of educational, scientific and cultural institutions, although the scheme as a whole is operated for the benefit of both individuals and institutions. Purchasers of Book Coupons need not apply personally to the distributing body but can, if they prefer, place their orders with local booksellers, who will themselves undertake all the necessary formalities.

Full details of the scheme and addresses of distributing agencies can be obtained from Lange, Maxwell & Springer Ltd., 41—45 Neal Street, London, W.C.2., or direct from UNESCO's Clearing House for Publications, 19 Avenue Kleber, Paris 16e, France.

FILED IN STACKS
8 Jul 54

Lange, Maxwell & Springer Ltd.

SCIENTIFIC, MEDICAL AND TECHNICAL BOOKSELLERS

take this opportunity to announce that they have established a special division within their organisation to handle exclusively the supply of Scientific, Technical and Medical literature to Industrial and Educational Research Organisations and Libraries

This division offers the following services:

- **Regular News Service** regarding newly published books and journals in all languages on Scientific, Technical and Medical subjects, contained in the LANGE, MAXWELL & SPRINGER BOOK NEWS sent free of charge on request
- **Supply of books and periodicals** on Subscription, published anywhere and in any language. Prices charged are at the official rate of exchange
- **Supply of Rare and Out-of-Print Books, Sets and Runs of Periodicals**
- **Translations of Foreign language Articles** undertaken
- **Hand-binding in our own bindery:** Speedy service at competitive prices
- **Books sent on approval if required**
- **Purchase or exchange** of surplus books and journals

We invite your inquiries, and particularly we invite you to visit our

SHOWROOMS at 138 SHAFTESBURY AVENUE, LONDON, W.C.2,

which are open from 9.30 a.m. to 6 p.m. on Mondays to Fridays, and from 9 a.m. to 12.30 p.m. on Saturdays

We shall be pleased to arrange for our Representative to call in order to discuss with you any problems you may have with regard to the supply of Scientific, Technical and Medical literature

LANGE, MAXWELL & SPRINGER LTD.

41–45 NEAL STREET, LONDON, W.C.2

Telephone: Temple Bar 1124

Printed by Universitätsdruckerei H. Stürtz AG., Würzburg